2

Feasibility of Using LODOX Technology for Mammography

Alyson Lease

Submitted to the Faculty of Health Sciences at the University of Cape Town in fulfillment of the requirements for the degree of Master of Philosophy in Biomedical Engineering.

Cape Town

August, 2001

Declaration

I, ALYSON LEASE, hereby declare that the work on which this thesis is based is my original work (except where acknowledgements indicate otherwise) and that neither the whole nor any part of it has been, is being or is to be submitted for any other degree in this or any other University.

I empower the University to reproduce for purpose of research, either the whole or part of the contents of this thesis in any manner.

Signature

Date

Abstract

The LODOX MP (Low Dose Digital X-ray Medical Prototype) X-ray Scanner, created by Debex Inc., is currently being clinically tested at the Groote Schuur Hospital and the University of Cape Town in South Africa. This system was implemented in June 1999 and has produced high quality full body digital images in the hospital's fast paced Trauma-Resuscitation Unit. In the high resolution mode, LODOX detects fine pulmonary detail and vascularity, thus suggesting that LODOX technology may also be used to identify breast cancer. An assessment and comparison of image quality and radiation dose was performed to determine the feasibility of using LODOX technology for mammography.

Image quality parameters examined for this assessment include beam quality (Half Value Layer), modulation transfer function (MTF), and detective quantum efficiency (DQE). LODOX half value layer was calculated at 40kV using techniques standardized in the literature. MTF and DQE measurements were modeled after the methods of Gransfors and Aufrichtig (2000). A basic comparison of scatter was done using Monte Carlo-generated equations specific to mammography and the LODOX scatter to primary ratio. LODOX absorbed dose measurements were calculated and compared using two general methods: exposure-to-dose conversion factors based on depth, and total energy imparted divided by mass. The mean glandular dose at various intensities (70 -125 mAs) was calculated based on entrance exposure.

At 40kV, the lowest possible LODOX energy setting, an average HVL of 1.59 mm of Al was measured (compared to 0.3-0.4mm of Al recommended for mammography). The LODOX modulation transfer function measured averages approximately 5-6% at 8-10 cycles per millimeter, and the detected quantum efficiency measured to approximately 25% at 1 cycle per millimeter, rapidly declining thereafter. Scatter to primary ratios for various breast diameters and thicknesses (0.29-0.59), calculated from methods in the literature (Boone and Cooper, 2000), were higher than the LODOX SPR value (0.2) measured previously (Booysen, 1998). The mean glandular doses calculated for a breast thickness of 4 cm at various intensities (ranging from

0.022 rad at 70mAs to 0.043 rad at 125mAs) were significantly less than the value designated by the American College of Radiology (0.3 rad per breast image). Compared to existing digital mammography systems (General Electric Senographe 2000D), LODOX is slightly less capable of transferring contrast. However, the proximity of LODOX MTF to an FDA-approved system suggests that LODOX technology may be suitable for a mammographic prototype with certain modifications. LODOX DQE values are higher than the screen-film system at very low frequencies ($\leq$ 1 cycle/mm), indicating that LODOX can detect more incoming photons with a lower radiation dose at a decreased spatial frequency. Standards for mean glandular dose set by the American College of Radiology are approximately 10 times the mean glandular dose delivered by a LODOX scan for a breast of a given thickness.

Image quality parameters show that LODOX technology, because it was built for general radiology, does not specifically conform to mammographic standards. The fundamental reason for this is the system's optimal energy range and beam hardness. From half value layer measurements, it was evident that the LODOX x-ray beam exhibits higher penetrability than mammographic systems, even at low energy. While hard x-rays are necessary for regular diagnostic radiography, low energy beams are preferred for mammography. However, with adjustments to the x-ray range and scintillator thickness, LODOX technology has considerable potential for imaging objects with lower attenuation differences, such as breast tissue. The extremely low radiation dose delivered by the LODOX-MP suggests that this type of technology would be optimal for detecting and diagnosing cancers in the sensitive tissue of the breast.

Acknowledgements

Enthusiastic thanks to a number of people who have served as the driving force behind the author and the research that follows.

Professor C.L. Vaughan, head of the Department of Biomedical Engineering, UCT, for his inexhaustible guidance as thesis supervisor.

Professor Steve Beningfield, head of the Department of Radiology, Groote Schuur Hospital, for his supportive counsel as additional supervisor.

Dr. Andre Booysen (LODOX Electro-Optical Engineer) and Herman Potgieter (LODOX Project Manager), both of DebTech, for their instruction and constructive advice.

Additional thanks to staff of Groote Schuur Hospital: Jan Hough, Department of Medical Physics for his radiological expertise and support; Gillan Bowie, Department of Radiology, for her instruction and use of the film densitometer and radiology films; and Dr. Egbert Herring, head of the Department of Physics, for his valuable imput. Thanks also to Professor Charles Slater of the Anatomy Department, University of Cape Town Medical School, for his cooperative assistance in anatomical considerations.

A special thanks to the staff and fellow students of the Department of Biomedical Engineering and African Medical Imaging, for their ideas and encouragement, especially the LODOX lab. My interval of research and study in South Africa has been exceptional due to the stimulating surroundings.

And finally, thank you to my family and Steve McIntosh, who have supported me from many miles away.

Table of Contents

List of Figures

List of Tables

Abbreviations

ACR	American College of Radiology
AGD	Average Glandular Dose
CC	Cranio-caudal
CT	Computed Tomography
DQE	Detective Quantum Efficiency
ESF	Edge Spread Function
FDA	Food and Drug Administration
H&D	Hurter and Driffield
HVL	Half Value Layer
LODOX	Low Dose Digital X-ray (System)
LSF	Line Spread Function
MLO	Medio-lateral Oblique
MTF	Modulation Transfer Function
NPS	Noise Power Spectrum
PSF	Point Spread Function
SID	Signal to Image Detector Distance
SNR	Signal to Noise Ratio
SPR	Scatter to Primary Ratio

Chapter 1

Introduction

To say that breast cancer is a major threat to the female population worldwide is a profound understatement. Until a cure for cancer is discovered, the best means of reducing breast cancer mortality lies in detection and treatment at the earliest possible stage. Mammography is the only universally accepted means of screening women for breast cancer. Although women may privately administer their own breast self examinations, tumours must first be large enough to be discovered, at which time they may already be fatal.

It is estimated that 1 in 4 of all South Africans will be affected by at least one cancer diagnosis in their lifetime. Breast cancer currently accounts for 9% of all cancers worldwide (Breast Cancer Worldwide, 2000). In the United States, 32% of cancer incidence and 18% of cancer deaths are from cancer of the breast (Huda and Slone, 1995). Although lower rates have been reported in African countries than Europe and North America, this may be a result of a smaller percentage of the female population being screened. No national screening programme exists in South Africa with the purpose of breast cancer detection. However, according to the Cancer Association of South Africa, breast carcinomas are currently the most common type of cancer among South African women (Cancer Association of South Africa, 2000).

Digital imaging reflects a current technological trend in medical radiology for a number of legitimate reasons. Reduced radiation doses, faster results, and increased image quality are just a few of the incentives for hospitals to implement digital imaging systems. Mammography, in particular, is the last field of radiology to become digital because it requires the most delicate compromise between high image quality and extremely low doses of radiation. Only one digital mammography system has been approved by the Food and Drug Administration (FDA) in the United States to date.

Low Dose X-ray (LODOX) technology is currently being utilized and tested as a means of providing safe and efficient quality medical images. LODOX's capability to produce high quality images, with exceptionally low radiation, suggests that this technology could be adapted for a dedicated mammography prototype. The crux of this thesis is to determine the feasibility of using LODOX technology for mammographic images, as well as providing recommendations that would enhance the performance of a LODOX mammography prototype.

The LODOX MP (Low Dose Digital X-ray Medical Prototype) X-ray Scanner, created by Debex Inc., is currently being tested and used in the Trauma Unit at the Groote Schuur Hospital in Cape Town, South Africa. This project will examine the image quality and radiation delivery of LODOX PPM to consider the feasibility of utilizing LODOX technology for digital mammographic imaging.

In the second chapter of this thesis, a general literature view of breast cancer and mammography systems is presented. This investigation includes an analysis of current digital mammography systems, and clarifies concepts regarding image quality.

The third chapter of this study explores image quality parameters with respect to LODOX technology. Beam quality, in terms of half value layer (HVL), noise, contrast, and resolution, will be evaluated.

The fourth chapter quantifies the radiation risk that LODOX delivers for breast imaging. The exposure, entrance dose, energy imparted, and effective equivalent dose are calculated from experimental measurements. The absorbed dose and absorbed glandular dose have also been analyzed and compared to the mammography dose requirements of the American College of Radiology (ACR).

The final chapter of this investigation addresses the necessary considerations for the implementation of LODOX technology in the field of mammography. The author also makes recommendations regarding future developments in LODOX-based mammography.

Chapter 2

Literature Review

2.1 Breast cancer

2.1.1 Brief anatomy of the breast

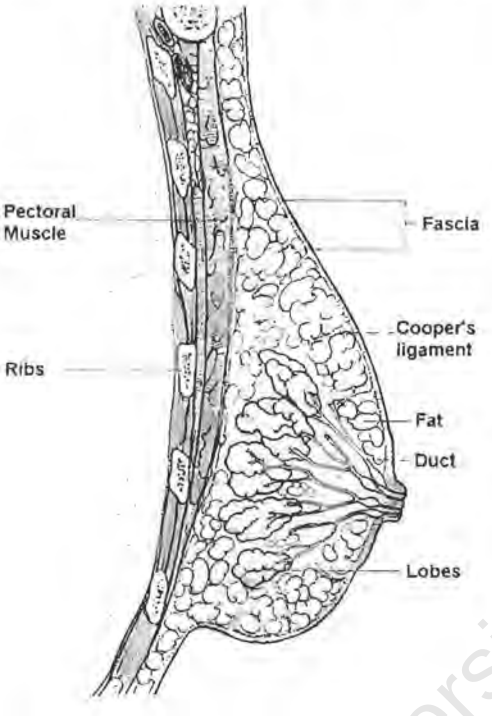

Figure 2.1: Illustration of breast anatomy, adapted from Andolina *et al.*, (1992).

The breast is composed of glandular and adipose tissue and surrounded by an outer layer of superficial skin (0.5 to 2.0 mm thick) and a bilayer of fascia. Below this lies a layer of subcutaneous fat, which may or may not be continuous with the adipose tissue between the glandular components. Glandular tissue, which is the accepted origin of breast cancer, consists of a number of ducts, each of which defines a segment or lobe of the gland. Between 8 and 20 ducts become superficial at the surface of the nipple. Directly interior to these openings are extensions of lactiferous sinuses, which transport milk during lactation. More interior to the chest, major ducts divide into numerous branches and terminate into lobules, blunt ending ductiles shaped like a bulbs.

A majority of breast is located between the second and seventh ribs, anterior to the pectoralis muscles. Vascular supply to the breast is via the lateral thoracic artery, and innervation originates predominantly from the cutaneous branches of the thoracic intercostal nerves. Lymphatic drainage of the breast is of particular concern because tumors in the lymph system have the potential to metastasize (spread to other organs). The bulk of breast drainage is to the axilla, and intramammary lymph nodes can be seen in about 5% of normal women by a mammogram. When a lymph node contains cancer it is treated with radiation or removed to avert tumour spreading or recurrence.

2.1.2 Aetiology

Environmental factors, as well as genetics are attributed to breast cancer incidence. External influences may include contact with chemicals (carcinogens) through inhalation or ingestion, or exposure to radiation that may alter DNA. In terms of genetic factors, women who inherit an abnormal gene are predisposed to subsequent breast cancer development. Some women with hereditary breast cancer have been found to retain a mutation or loss of tumor suppressor gene p53 on chromosome 17p (Malkin *et al.*, 1990). BRCA1 and BRCA2 (on chromosomes 17q21 and 13q, respectively) are other heritable genes that have been identified as instigators of breast cancer (Wooster *et al.*, 1994).

Breast cancer occurs as the result of two or more alterations in the chromosomal DNA of a cell. As an alternative to being corrected by typical DNA repair mechanisms, the damage is passed on to future generations of cells. Without this proliferation, mutations in the DNA would not become expressed. Eventually, unrestrained cell growth results when sufficient damage accumulates in particular genes. Multiple damaging events must occur at specific sites in the chromosome to generate prolonged existence of the cancer. If cells that replicate without inhibition gain access to the lymphatic and vascular systems, they acquire the ability to become metastatic. Early detection allows for the treatment of cancer before it reaches this fatal stage.

2.1.3 Classifications and diagnostic views

Figure 2.2: mediolateral oblique (MLO) view of a lesion. Source cited in text.

The most common breast tumour formations are mass lesions and microcalcifications. Microcalcifications (Figure 2.3) are specks of hydroxyapetite [$Ca_5(PO_4)_3OH$], with diameters as small as 100μm and originate in the gland ducts, often in clusters. Microcalcifications are associated with both benign and malignant cancer although there is an increased risk for malignancy based on the number, morphologic appearance, size, and distribution (Sickles, 1986). Contrary to previous thinking, recent studies have shown that clustering (more than 5 microcalicifications in an area of 0.5 x 0.5cm), is not always an effective way to diagnose malignancy (Park *et al.*, 2000). Larger mass lesions (Figure 2.2) are characterized by fine fibrillar structures that radiate from the mass or the presence of architectural distortion. Lesions are usually much larger and easier to detect and can grow to over 5 cm in diameter. The average size of a lesion is 2-3 cm, but at that time the five-year survival rate is only 60% (Wanebo *et al.*, 1974).

Figure 2.3: Cranio-caudal (CC) view of micro-calcifications. Source cited in text.

Two mammographic images are taken at different angles to allow for adequate visualization of the entire breast region. Although this doubles the radiation dose delivered to the breast tissue, two views have been proven to detect significantly higher cancers with a lower recall rate (Wald *et al.*, 1995). Published studies show missed detection rates up to 25% with a single view (Morrison *et al.*, 1998).

A medio-lateral oblique (MLO) view, Figure 2.2, can be taken at angles ranging from 30 to 60 degrees from the transverse line (Andolina *et al.*, 1992), while a standard cranio caudal (CC) image, seen in Figure 2.3, is taken in the transverse plane (parallel to the ground). The mediolateral oblique is the most useful projection of the breast (Kopans, 1998) because it allows the breast tissue to be pulled away from the chest wall using compression in the plane parallel to the pectoralis muscle fibres. This axillary region is the location of lymph nodes, where tumours have the opportunity to metastasize. Figures 2.2 and 2.3 were taken from the University of Southern Florida digital mammography database.
(http://marathon.csee.usf.edu/Mammography/ Database.html)

2.1.4 Incidence and early detection

Being female is the most notable risk factor for patients afflicted with breast cancer. Although breast cancer also occurs in men, less than 1% of cases are attributed to the male gender (Kopans, 1998). Other less obvious factors include early menarche, late menopause, nulliparity, or later age of first full term pregnancy. The incidence of breast cancer also increases with age. Likewise, either a previous history of breast cancer, or a first- degree relative (mother, sister, or daughter) history of breast cancer can also indicate a high-risk female. Incidence rates for different races may be related to culturally linked traits such as diet, hereditary patterns, or variations in socioeconomic status (Mettlin, 1999).

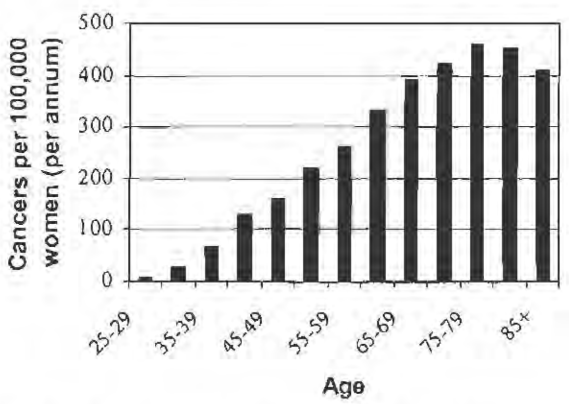

Figure 2.4: Breast cancer incidence severely increases with age. Data from Kopans, 1998.

Age is an important indication of breast cancer risk because unrestricted cell growth is projected to occur more often in women as they age because non-fatal DNA damage is less likely to be repaired. Breast cancer incidence is shown to increase substantially from as early as 35 (Figure 2.4). To facilitate early detection, women are recommended to have a base mammogram taken at the age of 40, and with a follow-up every 2 years. After the age of 50, annual mammograms are advised.

Until the causes of cancer are fully deciphered and resolved, early detection through screening is the main strategy for breast cancer mortality reduction. According to Kopans (1998), "Mammography is the primary breast imaging technology and the only system that has been validated for screening." Undeniably, early cancer detection through mammography screening is recognized as the primary cause of drastic reductions in breast cancer mortality (Feig, 1995).

Study (dates)	Screening frequency	Mortality
HIP, NY (1963-69)	12 months	-23%
Malmo, Sweden (1976-86)	18-24 months	-49%
Kopparberg, Sweden (1977-85)	24 months	-27%
Edinburgh, Scotland (1979-88)	24 months	-22%
Stockholm, Sweden (1981-85)	28 months	+4%
Gothenburg, Sweden (1982-88)	18 months	-24%

Table 2.1: Compilation of randomized clinical trials of women aged 40-49, illustrating drastic reductions in breast cancer mortality. (Adapted from Feig, 1995.)

2.2 Mammography

The first reproducible technique for radiographically imaging the breast using film-screen mammography was described in 1960 at the M.D. Medical Hospital in Houston, Texas (Egan, 1960). By the mid -1960s, the first dedicated mammography unit was created in France, and similar systems are still constructed and utilized today. Film-screen mammography is currently the gold standard for breast cancer diagnosis and detection around the world. With the advent of digital technology, digital mammography has become possible. Early in 2000, the FDA approved the first digital mammography system to be used for routine breast cancer screening. However, despite these advances, many developing countries, such as South Africa, lack a national screening programme for the detection of breast cancer.

2.2.1 Equipment

In a mammography system, an x-ray tube must create radiation with enough energy to penetrate the breast but not so much as to prevent adequate contrast and spatial resolution. The radiospectrum of x-rays is determined by both the target/filter combination of the tube and the peak kilovoltage setting on the x-ray unit. A filter eliminates the non-useful portion of the x-ray, thus reducing unnecessary radiation exposure. The limit of the absorption is specific to the filter, and variations of molybdenum, tungsten, and rhodium are commonly used for both the target and the filter due to their favourable radiation peaks. Breast density and thickness must be taken into account when determining the target and filter because denser breasts require higher energy radiation. However, energy that is too high reduces the soft tissue contrast and is not favored for imaging breasts of containing more fat and connective tissue. A standard screen-film mammography system (Figure 2.5) illustrates the primary mechanical

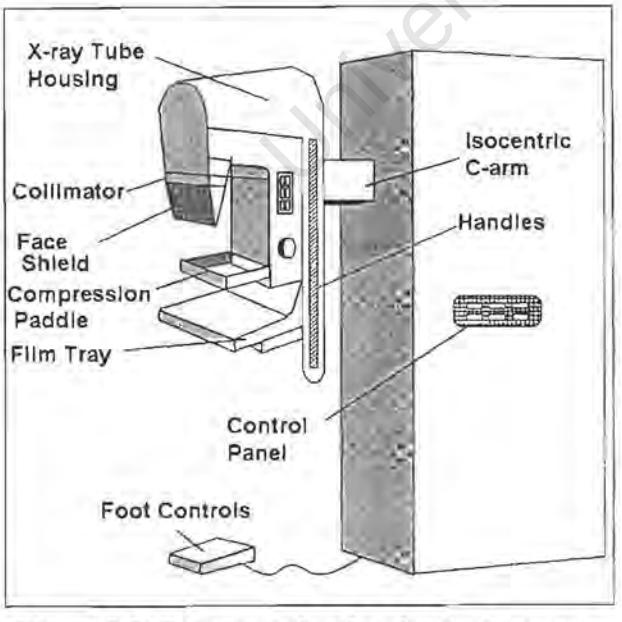

Figure 2.5: Components of a standard screen-film mammography unit (Andolina *et al.*,1992).

components.

The breast is exposed to a spectrum of x-rays, some of which are scattered while others are transmitted through the tissue. The transmitted x-rays pass through a grid composed of upright lead strips, which allows only parallel radiation to pass, whilst the scattered radiation is absorbed. The grid also moves perpendicular to the incident x-rays to ensure that the lead strips do not become a permanent fixture on the resultant image. The efficiency of the grid depends on the height and spacing of the strips. Conventional mammography techniques that use grids require 2 to 2.5 times more exposure than non-grid techniques (Haus and Yaffe, 2000). However, since grids drastically reduce the effects of scattered radiation, they are used almost universally for nonmagnification views.

A compression paddle also reduces the proportion of scattered radiation by restricting the thickness of the breast to a uniform width. Breast compression results in higher image contrast and a reduction in geometric unsharpness. Compression also restricts a patient's motion, which permits a sharper image through a shorter exposure time. Radiation dosage is reduced because a thinner breast requires less radiation to achieve the same film optical density. Flattening the breast also decreases over-penetration in the thinner anterior tissues and under-penetration of thicker posterior tissues and allows better visualization of lesions by reducing superimposition of breast tissue. However, compression pain is the largest patient complaint due to the sensitivity of breast tissue.

Certain specifications for mammography equipment contribute to safe high-quality imaging. Many important aspects of x-ray equipment include mechanical considerations, the x-ray tube focal spot and spectrum, generator performance, collimation, scatter rejection, and the automatic exposure control. Equipment recommendations set forth by the American College of Radiology Focus Group and the European Commission for Public Health clarify the optimal imaging system design, taking into account the assembly, quality, and alignment of the equipment, as well as the technique used in performing mammograms (Yaffe *et al.*, 1995). Whilst these guidelines address all screen-film stipulations (such as detector regulations, and film quality), they pertain to most aspects of a digital system as well.

2.2.2 Screen-film Mammography

Analogue-based mammography is currently the most common method used to screen patients for existing cancers. Breast tissue is highly sensitive to radiation exposure. When administering a mammogram the emitted dose must be kept exceedingly low because breast cancer screening requires recurrently exposing large populations of women to radiation.

Mammograms must also maintain a lower dynamic range of high contrast than chest or bone radiology because small differences exist in the soft tissue density of the breast. As a result, the relationship between x-ray exposure, image density, and contrast, is a delicate one. The Hurter and Driffield curve illustrates the narrow exposure latitude (dynamic range) on a screen-film system under given conditions (Reynolds, 1999). High contrast in the intermediate-density regions of the breast is only plausible with less contrast in the shoulder and toe of the curve (the fatty tissue and the glandular tissue, respectively).

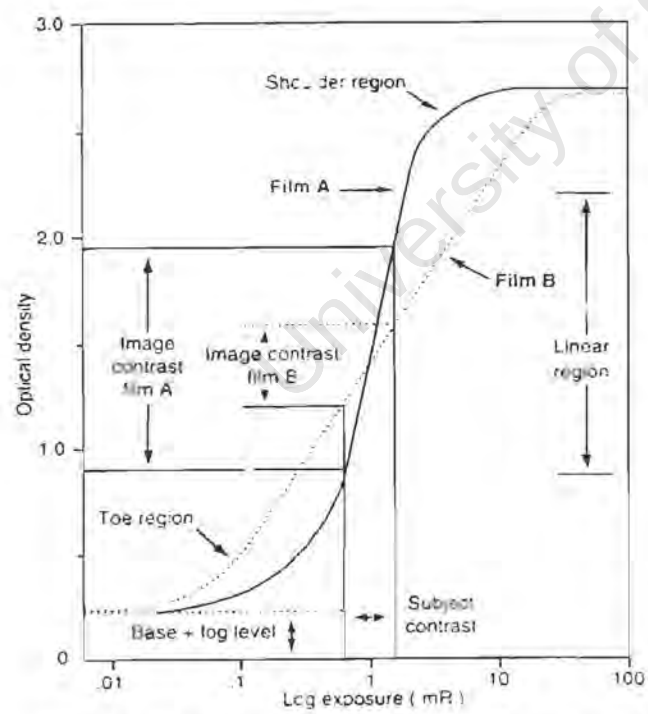

Figure 2.6: Hurter and Driffield curve (Huda and Sloan, 1995) illustrating the characteristic relationship between exposure and optical density in screen-film systems. Film A exhibits higher contrast while Film B maintains wider exposure latitude.

While the standard use of mammography screening is responsible for lower breast cancer mortality rates in the United States and Europe, screen-film mammography is not infallible. According to sources in the literature (Moskowitz, 1995; Huda and Sloan, 1995) screen-film mammographers miss approximately 10% of all cancerous tumours. This large percentage is partially a result of limitations in image quality that obscure the radiologist's view of architectural distortions and microcalcifications.

2.2.3 Secondary Digitization

Advances in digital technology have made it possible to scan analogue-based images into digital format. Some benefits of secondary digitized images include easy transportation (telemammography) and storage. Digitization also facilitates the analysis of digital mammograms on a computer monitor, using distinct and uniform algorithms instead of fallible human evaluation. Likewise, it is possible to use algorithms to locate areas that are potentially malignant, thus combining both computer and human analysis. However, since the same amount of information available from a film is transferred to the digital display, there is no increase in spatial resolution. Some information is actually lost in the digitization process so it is possible that a secondary digital mammogram has less information than its analogue counterpart. As a result, imaging characteristics of the film, such as film gradient, can limit the subject contrast and the response of film to light is usually characterized by the H&D sigmoidal curve mentioned beforehand that narrows screen-film exposure latitude (Reynolds, 1999). However, contrast and brightness can be adjusted on a monitor.

2.2.4 Primary Digitization

Primary digital x-rays immediately convert light photons to an electronic signal, without intermediary film processing. This usually involves a demagnifying fiberoptic coupling device and a detector, which collects the signal. After converting the x-ray signal to digital form, the detector quantizes the electronic signal into one of 2^n intensity levels, where n is the number of bits of digitization. The number of bits of digitization determines the number of image signal levels; since n is usually equal to 12 or 14, the number of signal levels is thus either 4096 or 16384. This digitized representation is either received by multiple sub-elements of a detector, or the output signal from a continuous detector is divided to represent smaller visual areas. This form of image acquisition, termed *spatial sampling*, facilitates the electronic digestion of large amounts of digital data. These signals are stored and processed in a computer and the resulting image can be displayed on a monitor or printed on film.

2.2.5 Advantages of Digital Mammography

Image quality in digital systems is equivalent to or better than screen-film quality. Contrast resolution is enhanced in digital systems because electrical output is directly proportional to the transmitted x-ray intensity throughout the breast, even in dense regions. As noted, the response of film to light is characterized by a sigmoidal curve that limits contrast in fatty regions and highly dense fibroglandular regions. Digital images have a wider dynamic range, with a linear response of 1000:1, compared with 40:1 for screen-film systems (Feig and Yaffe, 1998). Likewise, lower image noise is

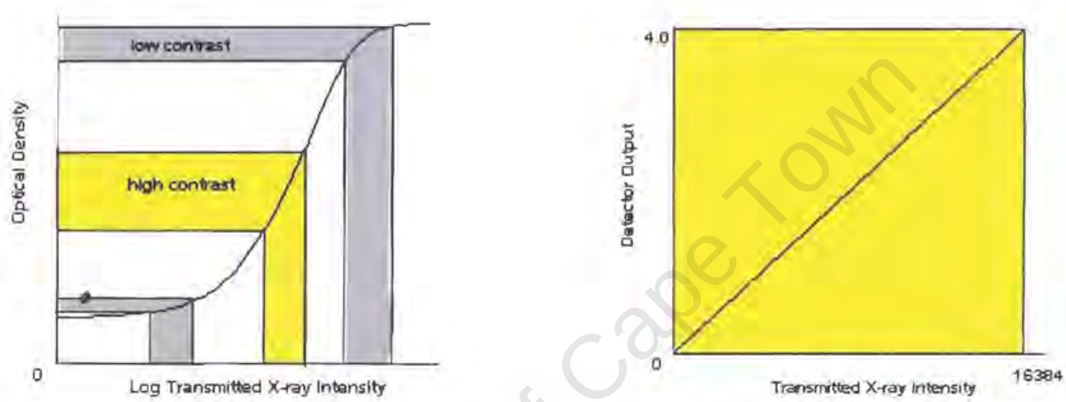

Figure 2.7a and Figure 2.7b: A comparison of the high contrast regions of film-screen and digital imaging. Figure 2.7a is also referred to as a Hurter and Driffield (H&D) curve.

present in digital x-rays, partially due to the lack of film.

Digital images can also be manipulated and enhanced because image acquisition, storage, and display are separate operations. Consequently, variant versions of the same image can be created at different brightness and contrast settings. Areas of interest can be enlarged and scrutinized, making the need for supplemental views unnecessary, thus eliminating a patient's additional exposure to radiation. Contrast and brightness can also be adjusted, making abnormalities in dense tissue easier to detect.

Film development severely hinders the rapid display of images, while digital images are almost instantaneous. As a result digital imaging is currently used in breast treatments requiring on-the-spot images (Whitlock *et al.*, 2000). The implementation of full field digital mammography in select Canadian clinics has reportedly increased throughput and productivity. According to reports, clinics can obtain two times the exam volume over their screen-film method (Klucas, 2000). The reduction in recall rates also reported reduces the radiation dose from supplementary exposures. Recall rates are reduced because breast-positioning errors in imaging can be corrected on the spot.

For mammograms, time efficiency translates into cost effectiveness. Presently digital systems are more expensive than their analogue counterparts; costing between $300,000 and $500,000, compared to $75,000 to $100,000 for a regular film machine (Harris, 2000). However, digital systems eliminate the cost of film itself as well as processing and storing the images. Faster patient processing over a shortened period of time either generates greater revenue or lessens a clinic's cost of upkeep. Other economic benefits include a reduced costs associated with film management, because film retrieval and archiving is an expensive, labour-intensive expenditure.

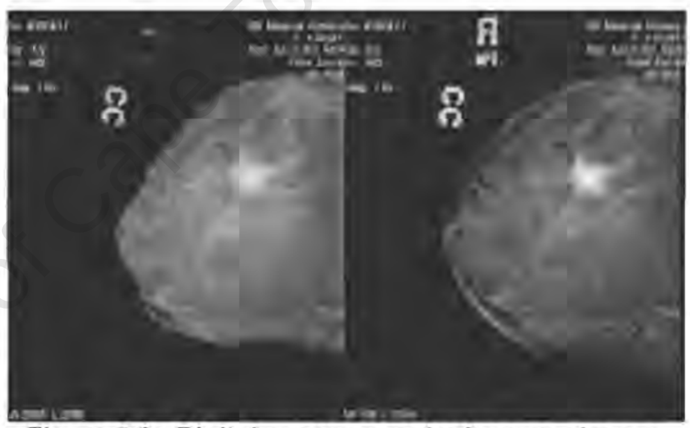

Figure 2.8: Digital mammography images show a right CC view of the breast before and after image reconstruction. (Source: GE Medical Systems, http://www.gemedicalsystems.com/rad, 2000)

The first attempts to detect and classify breast abnormalities using computers were administered as early as the 1970s (Ackerman and Gose, 1972; Spiesberger, 1979). Currently, computer-aided detection and diagnosis in mammography are in the early stages of clinical use. Computer analysis of mammographic images involves two phases, image processing (computer vision) and interpretation (artificial intelligence), which can be intermeshed within algorithms. In processing, important image features are commonly enhanced while those of little interest are de-emphasized using techniques such as image subtraction and segmentation. Bayesian image estimation (BIE) has been proven to advance image processing by reducing scatter content and improving the contrast-to-noise ratio (Baybush and Floyd, 2000). Artificial neural networks can then identify relationships between input and desired output parameters to detect and characterize abnormalities. Likewise, rule based methods (Nikishikawa *et al.*, 1995), discriminate analysis (Bankman *et al.*, 1993), and fuzzy logic (Cheng *et al.*, 1998), are different forms of artificial intelligence under investigation.

The sensitivity of the system, as well as its specificity, and the nature of the cases in its reference database, are the primary factors that effect the success of a computer-aided detection system. Studies suggest that significant differences exist in radiologists' preference for algorithms used to detect masses versus microcalcifications (Sivaramakrishna *et al.*, 2000). However, computer aided diagnostic algorithms have outperformed general radiologists in characterizing lesions as benign or malignant (with sensitivities for malignancy as high as 100% described) (Vyborny *et al.*, 2000).

Electronic storage devices, such as optical disks, facilitate the extended storage of digital image information. Picture archiving and communications systems (PACS) are based on a dedicated computer which can access data stored in digital image processors and transfer it at high speeds to archival storage media or other computer systems. Digital format facilitates the transport images (*i.e.* telemammography) between physicians or institutions eliminating lost or damaged film copies of mammograms. This also facilitates expert radiological consultation in any location with a necessary linked connection. While a compressed mammogram may not preserve the same image quality of its original, certain amounts of data compression (up to 101:1) can be maintained without the degradation of radiological quality with respect to detecting masses. According to Good *et al.* (2000), mammogram data compression does cause degraded observer performance in locating smaller details such as those necessary to define microcalcifications.

2.3 Image Quality

The literal image *quality* of a mammogram is an indistinct concept, indicating the clarity with which a radiologist can read the image. Thus, higher image quality should indicate a higher percentage of tumours detected and diagnosed properly. However, it is difficult to define the exact relationship between physical image properties (*i.e.* contrast, resolution, and noise) and the ability to detect and diagnose features. As a result, image quality is usually based on technical image attributes, such as contrast, spatial resolution, image noise, signal-to-noise ratio, and the absence of artifacts (Vyborny and Schmidt, 1994).

2.3.1 Contrast

Radiographic *contrast* refers to the magnitude of the signal difference between the structure of interest and its surrounding area. Contrast in a screen-film mammogram is defined as the optical density difference between corresponding areas on the processed film. For a digital system, contrast is quantified as the relative brightness difference between two areas in an image displayed on a monitor. Total radiographic contrast is dependent upon both the *subject contrast* and the *receptor contrast* of the system (Haus and Yaffe, 2000).

Figure 2.9: Illustration of the dependence of image performance on radiographic contrast.

Subject contrast defines the difference in x-ray exposure to the image receptor transmitted through adjacent parts of the breast. For example, microcalcifications and marginal characteristics of soft tissue masses illustrate different x-ray attenuation properties than the surrounded tissue area. These absorption differences are affected by the distinct qualities of the lesion and surrounding breast tissue, such as density, thickness, and atomic number. The spectrum of x-rays used in the mammogram (i.e. the *radiation quality*) and scattered radiation also affect the subject contrast. When scattered x-rays or excess high energy x-rays escape the breast and are recorded by the image receptor information content of the mammogram decreases because scattered radiation adds noise and reduces the signal to noise ratio of the image.

Receptor contrast is more problematic for screen-film mammograms than digital images because properties of the film often determine the magnitude of image differentiation. Film contrast determines how the optical density pattern on the film results from the received x-rays. In digital mammography the stored image reflects the subject contrast because its signal is directly (or logarithmically) proportional to the amount of radiation transmitted through the breast (Figure 2.7b).

2.3.2 Spatial Resolution

Spatial resolution defines the competence for recording fine detail – low spatial resolution results in coarser detail. When the structural boundaries of an image are spread into its surroundings, the resolution of the image is degraded. This spreading, known as *blurring*, can be caused by any combination of motion, geometric, or the receptor influences. The Motion Transfer Function (MTF) is a numerical measure of spatial resolution because it describes the ability of a system to transfer the contrast (modulation) of a structure to its final recorded image. A system with an MTF of 0.1 necessitates that 10% of the inherent contrast of the object has been retained on the recorded image. *Limiting spatial resolution* is defined as the frequency at which the MTF reaches a certain value (4-5%)(Rossman, 1963).

Motion blurring, often caused by prolonged exposure time, results from the movement of the breast during the exposure period of the imaging process. Exposure periods less than two seconds, along with compression, are desired for the reduction of motion blurring. Motion blurring for digital systems is also dependent upon the duration of exposure. A scanning system requires longer overall exposure although only part of the breast is exposed to x-rays at any given time. Therefore, motion can cause the accumulation of false signals between the sections imaged before and after the movement.

An image's *geometric blurring* is effected primarily by the depth, intensity distribution, size, and shape of the x-ray tube focal spot. The focal spot creates a shadow of any structure within the breast that increases with the degree of magnification between the structure and the receptor. When the shadows overlap, the result is blurring. Shadow size depends upon the size and shape of the focal spot, as well as the *SID* (source to image receptor distance). Maximizing

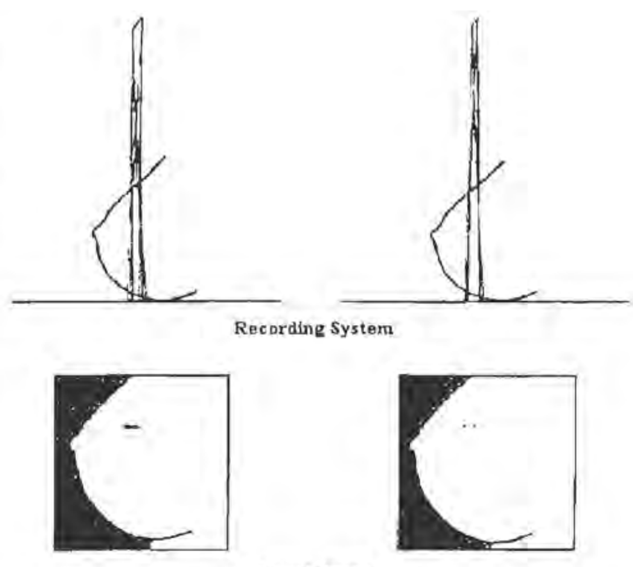

Figure 2.10: Illustrating how a small focal spot reduces geometric blurring (Adapted from Haus and Yaffe, 2000)

the distance between the focal spot and object, and minimizing the distance between the object and image receptor reduces geometric blurring.

Receptor blurring occurs distinctly in screen film systems and digital systems. For screen-film radiography, light is usually spread by a screen before it has a chance to be recorded. Phosphor layer thickness, phosphor particle size, dye and pigment content in the screen (causing light absorption), and screen film contact are properties of the screen that influence blurring (Haus, 1990). In digital systems, receptor unsharpness results from signal diffusion between elements, the active area of each element, and the pitch (center to center spacing) between elements (Haus and Yaffe, 2000).

2.3.3 Noise

When a radiograph that is given uniform x-ray exposure illustrates variation in random optical density, the phenomenon is termed *noise* or *mottle*. Noise is generated by factors both before and after an image is recorded, hence screen-film and digital systems maintain some similar noise sources. Noise resulting from film grain and film processing artifacts is restricted to screen-film systems, while quantum mottle and x-ray-to-light conversion noise affect digital mammography systems as well.

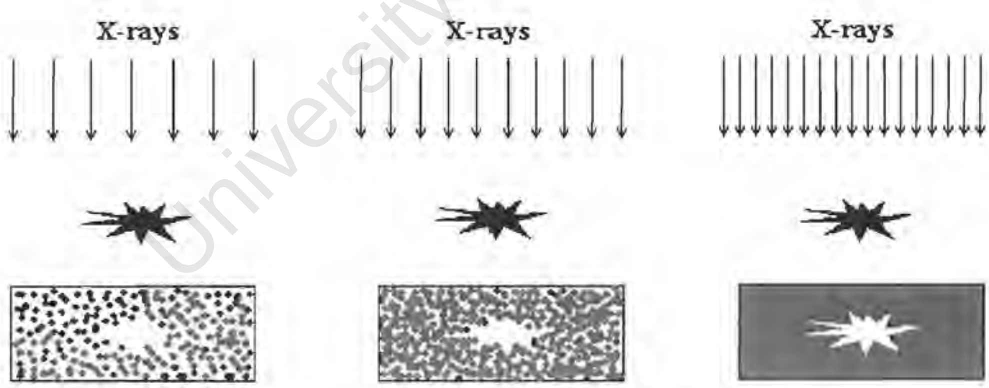

Figure 2.11: Quantum mottle results from random spatial variation of photons and decreases as the number of photons is maximized.

The x-ray quanta absorbed in the image receptor exhibit random spatial variation known as *quantum mottle*. When additional x-rays form an image, this quantum noise is reduced because the fluctuation in the image relative to useful signal decreases and thus noise diminishes. Unfortunately, fewer x-rays must be used in faster (more sensitive) systems that increase conversion efficiency, making quantum noise an inevitable consequence. Noise resulting from the screen structure and film increase with the sensitivity of the screen-film materials, thus limiting the precision of its technology. Noise that results from x-ray-to-light conversion is a product of fluctuations of the amount of light produced in the screen when an x-ray quantum is absorbed; this type of mottle is a statistical fluctuation. In digital systems, variations in receptor sensitivity can created a fixed pattern of noise. *Flat fielding*, recording an image of a uniform field of x-rays as a correction control, is used to subtract fixed digital noise.

2.3.4 Artifact

Artifacts complicate the ability to detect and characterize lesions because they either obscure growths that are actually present or stimulate false lesions. In both screen-film and digital systems artifact can result from preprocessing – the x-ray source, beam filter, compression device, breast support table, screen, and grid, are all sources of artifact that have been documented in screen-film mammograms. However, for screen-film systems, the film, processor, and darkroom can add artifact distinct for its latent film. Digital artifact is detector specific because images that are stitched together out of subimages contain multiple recording elements, each of which is subject to nonuniformities and miscalibrations. Errors in scanning can also augment the possible sources for digital artifact.

2.4 Radiation Factors

The American College of Radiology (ACR) Mammography Accreditation Program requires a mean glandular dose of 3 mGy (0.3 rad) or less for a breast phantom image 4.5 cm thick. Other radiation measurements, such as exposure, entrance dose, effective equivalent dose, and the energy imparted to the breast, are useful for deriving and comparing absorbed (glandular) dose values. These are defined and discussed in Chapter 3.

2.4.1 X-ray tube

The difference in voltage created across an x-ray tube is measured in kVp (kilovolts peak), which is the maximum voltage that crosses the x-ray tube during a complete waveform cycle (Huda and Slone, 1995). The electronic potential is measured in kVp rather than kV because it can be described as pulsating and represents the maximum or peak kilovolt value. The electrons that arrive at the anode can theoretically utilize all of this potential energy for conversion into x-rays, and the kinetic energy of the x-rays leaving the tube is expressed in kiloelectron volts (keV). Thus, if the voltage of the x-ray tube is 25 kVp, and the electrons can arrive at the anode with 25 keV of kinetic energy, and this energy is now available for transfer into electromagnetic energy in the form of photons.

In a conventional full wave rectified generator, the electrical potential can be pulsed from zero to 120 times per second. Since the waves are rectified, the electric potential is zero (ceasing to flow) 120 times per second, and the electric potential is at its maximum 120 times per second. A multiphase generator is necessary for imaging because it increases the number of electrons that reach the anode with a maximum accelerating voltage, thus decreasing the variation in electron energies.

Characteristic X-ray Energies for Common Anode Materials

Anode	Z	K-Shell	L-Shell
Copper (Cu)	29	8.0-8.9	0.9
Molybdenum (Mo)	42	17.4-19.6	2.3-2.6
Tin (Sn)	50	25.0-28.5	3.4-4.1
Tungsten (W)	74	58.0-67.2	8.3-11.3

Table 2.2: Selected characteristic x-ray energies (Taken from *Review of Radiological Physics*, Huda and Slone, 1995). The LODOX anode is composed of W.

Characteristic radiation results when electrons from the cathode strike and eject the inner electrons of the target material on the anode (*i.e.* the photoelectric effect). The vacant inner orbits of the target atoms are then filled by outer electrons and release a specific energy. As a result, energy of the x-ray produced is equivalent to the difference in binding energies of the two orbits and thus dependent upon the atomic number of the target material.

Each anode material emits characteristic radiation of a particular energy range, as illustrated in Table 2.1. K-shell electrons are only emitted when the incident electrons have an energy greater than the binding energy. L-shell x-rays have characteristically low energy and for normal radiographic systems, are usually absorbed by the window of a tube. A tungsten anode (like that of the LODOX-PPM x-ray tube) does not release K-shell electrons until the applied tube voltage exceeds 70 kV because the K-shell binding energy is 69.5 keV. As a result, K-edge filters must be employed to reduce the high energy photons which would degrade image contrast. Thus, at energies below 70 kV, electrons striking a tungsten anode interact via white radiation, or *bremsstrahlung*.

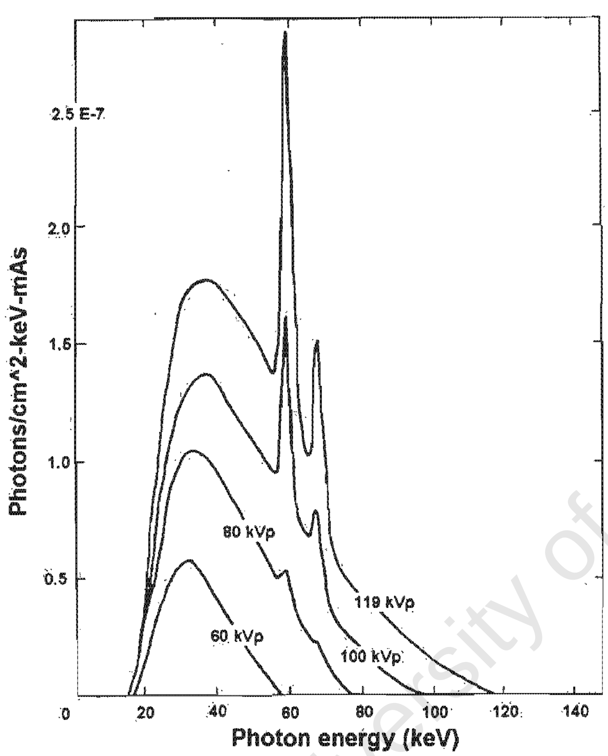

Figure 2.12: Tungsten spectral data taken from Yaffe *et al.*, 1976. The spikes represent the characteristic radiation peak and the gradual prominences are caused by bremsstrahlung.

A majority of x-ray generation is a result of Bremsstrahlung, or 'breaking' radiation, which results from interactions between incident electrons and the target atom nuclei. The positive charge of the nucleus attracts the negative electron, causing it to decelerate and change direction. Consequently, energy is given off as a photon, which is dependent upon the incident electron energy and its amount of deflection. It is possible for incident electrons to have multiple interactions with the target atoms and give off their energy in many stages, thus producing a continuous x-ray *spectrum*. Bremsstrahlung production of x-rays will increase with an anode that has larger atomic number (Z), or with accelerating voltage (kV).

2.4.2 X-ray interaction with the body

When an x-ray strikes human tissue, its energy is either absorbed or transmitted. If the energy is absorbed, biological damage results at an atomic level. Initially, a photon strikes and displaces an electron in the body tissue. This releases scattering of radiation and a mobile electron, which causes ionization, excitation of atoms, and the breakup of molecular bonds. Most of the electron's energy dissipates in the body as heat, and the interactions that occur produce firstly chemical, and then biological damage as a result. Some high speed electrons may also strike a nucleus and create bremsstrahlung (Johns and Cunningham, 1983). Three distinct tissue interactions are defined below, and the percent of interactions that occur by each process are listed in Appendix D.

Coherent scatter is referred to as unmodified scatter because it involves no loss in energy. When the incident photon strikes the electrons of an atom they become excited and vibrate. These vibrations of charged electrons result in radiation of the same frequency as the incident photon, usually in a different direction. Unlike other x-ray interactions, no energy is converted into kinetic energy because the photon is merely scattered. Coherent scatter occurs mainly in the forward direction, which can result in the slight broadening of the angular width of a beam (Johns and Cunningham, 1983).

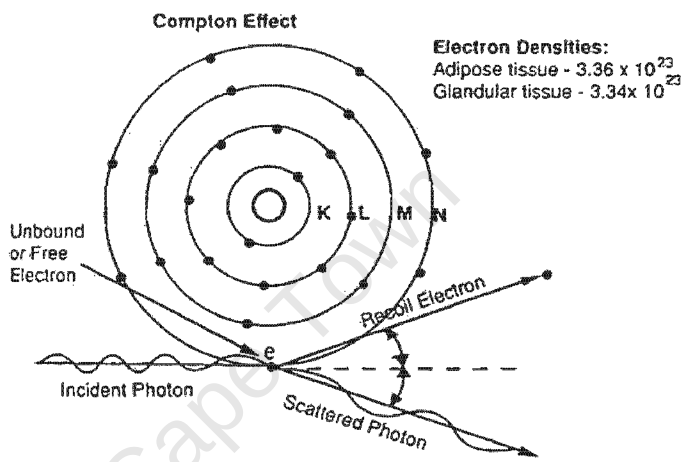

Figure 2.13: Illustration of the Compton Effect, from Andolina *et al.*, 1992.

The *Compton effect* produces scattered photons as a result of photon and electron interactions. When a photon collides with electrons that are free or loosely bound to an atom, it releases the electron from its outer shell. The radiation that is given off, in the form of a secondary photon, maintains the energy difference between the incident photon and the amount of energy required to remove the electron. The new photon retains only a portion of the initial photon energy, and may undergo more collisions, giving off more energy as it travels through the body. The Compton effect is dependent upon electron density. The electron densities of fat and glandular tissue share greater similarity (3.36×10^{23} electrons/g and 3.34×10^{23} electrons/g, respectively) than glandular tissue and dense bone (800mg/cm^3 hydroxyapatite) (4.89×10^{23} electrons/g). Therefore, there is less contrast differentiation in mammography than seen in general radiography. In either case, image quality is finest when the Compton effect is minimized or, if possible, eliminated.

X-rays produced by the *photoelectric effect* are also dependent upon the material being irradiated. When photons from the x-ray source interact with the atoms of the material, an inner shell electron is ejected in the form of a photoelectron. The incident photon then disappears because all of its energy has been transferred to the ejected photoelectron and the resulting hole in the electron cloud is filled by an outer shell electron, which liberates radiation characteristic to the target material. The atomic number of the irradiated material determines the energy of the x-rays produced, as well as the probability of the photoelectric effect occurring.

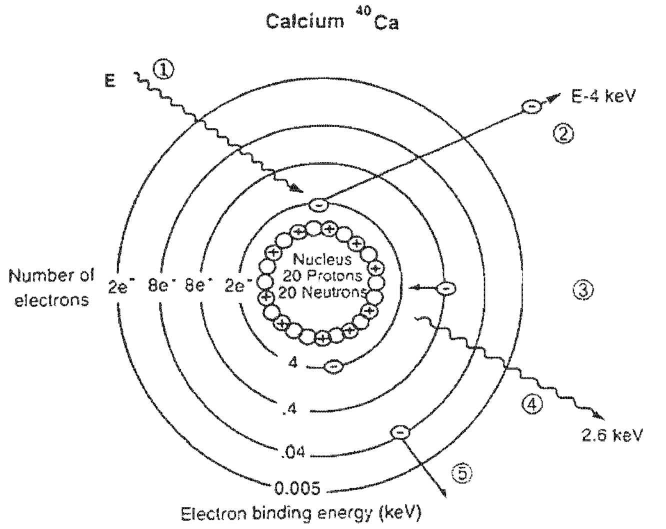

Figure 2.14: Illustration of the photoelectric effect on a calcium atom, adapted from Huda and Slone (1995).

Statistically, the photoelectric effect is most prone to occur when the energy of the incident photon is greater than, but close to, the binding energy of the orbital electron (Curry, 1990). A higher atomic number (Z) also ensures the possibility of a photoelectric interaction. This probability is proportional to the cube of the atomic number thus small increases in Z result in exponential photoelectric interactions (Johns and Cunningham, 1983). For diagnostic purposes, the photoelectric effect creates contrast between structures composed of dissimilar atoms. For example, calcium (Z = 20) in the bones has the probability of photoelectric interaction that is approximately 18 times higher than structures like muscle or tissue that contain large quantities of hydrogen (Z = 7.6).

2.4.3 Breast density dependence

Photoelectric absorption, along with the Compton effect, are the significant sources of x-ray absorption in soft tissue below 50 keV (Johns and Cunningham, 1983). Since breast tissue is usually imaged with x-ray energies between 20-40kVp, the small difference in atomic numbers of fat and tissue (5.9 and 7.4, respectively) play an important role in the transmission of x-rays. As the photoelectric effect is dependent upon atomic numbers, the composition and density of the substance being irradiated effects the radiographic quality of the image. For mammography, the low inherent contrast of breast tissue is enhanced by photons with lower energies. X-rays with high energy illustrate decreased information because transmission is related to the ratio of absorbed and unabsorbed photons.

To penetrate through larger, denser breasts however, an increase of kVp must be used. These denser structures result in beam hardening because x-rays are filtered as they pass through the tissue. Lower energy x-rays are absorbed and never reach the film, while higher energy x-rays have a decreased amount of information. As a result, contrast diminishes because tissues favor the transmission of higher energy x-rays.

2.5 Preliminary LODOX Considerations

The LODOX MP (Low Dose Digital X-ray Medical Prototype) X-ray Scanner, created by Debex Inc., is currently being tested and used at the Groote Schuur Hospital in Cape Town, South Africa. This system was implemented in the hospital's Trauma Unit in June of 1999 and has produced adequate full body images in the low resolution mode, as well as fine pulmonary detail and vascularity at modes of higher resolution

Figure 2.15: LODOX-MP X-ray Scanner, created by Debex, and based in the Trauma Unit at Groote Schuur Hospital in Cape Town (Beningfield *et al.*, 1999). Additional system information is given at http://www.lodox.com/

as well as fine pulmonary detail and vascularity at modes of higher resolution (Beningfield *et al.*, 1999).

The worldwide mammography market was predicted to surpass the $500 million mark by the year 2004 (Klucas, 2000). As of July 2000, four unique styles of digital mammography systems were being tested for commercial use. These are described in Appendix E. Since then, other similar full field digital mammography systems have been researched and developed for the prospective market although, only one has achieved full FDA approval. Comparative studies of full-field digital mammography and screen-film mammography for cancer detection have shown no difference in cancer detection rate (Lewin *et al.*, 2001). However, CAD applications, telemammography, and increased efficiency are still additive benefits of full-field digital systems.

To consider using LODOX or any system for mammography, certain aspects specific to breast imaging must be fulfilled (Kopans, 1998).

1) Extremely fine structures (microcalcifications and fibrotic strands) with sizes of about 100μm and only slight differences in density of surrounding tissue must be visible with high contrast, resolution and low image noise.
2) The imaging system must possess a wide object range to permit the visibility of areas of greatly varying density.
3) Examination by this system should involve the minimum dose of radiation sufficient to produce an image of acceptable quality, due to the sensitivity of mammary tissue to radiation.
4) The entire body of the gland must be imaged, with optimum standard positioning. Likewise, the knowledge and application of additional views must be available.

LODOX technology provides fast, high quality images with low doses of radiation. As a result, its feasibility for mammographic imaging is addressed in this thesis with respect to image quality and radiation dose.

Chapter 3
LODOX Image Quality

3.1 Introduction and Objective

An assessment and comparison of image quality was performed for this study to determine the feasibility of LODOX technology for mammographic imaging. Although the primary imaging function of the LODOX MP is trauma, its exceptional image quality suggests that LODOX technology may also be used to examine breast tissue.

Bone and tissue attenuate x-rays over different ranges of photon energy and intensity. However, using the current system one can distinguish certain tissue features, suggesting that the image quality is adequate for breast cancer diagnoses. In the high resolution mode, fine pulmonary detail and vascularity are visible. As a result, a primary objective of this study was to compare imaging parameters in order to determine what aspects of LODOX technology would have to be altered to create mammographic images for diagnosing breast cancer (*i.e.* comparable to that of film-screen images).

3.2 Beam Quality – Half Value Layer

The quality of an x-ray beam can be quantified in terms of *half value layer (HVL)*. HVL measures the thickness of a standard material required to reduce the beam to half its exposure value measured in Roentgen (Johns and Cunningham, 1983). At higher energy x-rays (120-400 kV) HVL is specified in mm of copper, and for energies below 120 kV mm of aluminum are used. HVL is a sufficient measure for specifying the biological effects of x-rays because image receptor sensitivity varies with HVL (Stanton *et al.*, 1984). Thus the half value layer of a system is also used in measuring dose (Chapter 4) because it quantifies characteristic beam hardness.

Filters are used to remove unwanted low energy x-ray beams that increase the amount of dose delivered to a radiated area. This occurs because soft x-rays (x-rays low in energy) can be absorbed by tissue without reaching the film. The radiation delivered to the patient by these low energy beams does not produce useful image information. By varying the filtration, x-rays of particular energies are not allowed to pass through to the detector. The amount of aluminum filtration required to reduce the image by half is an indication of the beam energy, or penetrability. X-rays of different energies (produced by the same x-ray tube) will demonstrate different HVL values because the penetrability of the beam changes. Thus, a higher x-ray energy beam should exhibit a thicker HVL measurement because the beam is harder.

By determining the HVL of an x-ray source, one can derive the energy imparted to a patient (Gkanatsios and Huda, 1997), or the absorbed radiation dose (Doi and Chan, 1980). With knowledge of the beam quality and the dose at which the beam enters the breast (skin entrance dose), resultant radiation can be calculated for an average breast composed of 50% glandular and 50% adipose tissue. For example, with an average breast of 4cm thickness, an HVL of 0.3mm of Al, and an entrance dose of 370mrad, the average glandular dose to a breast is 60mrad (Kopans, 1998).

3.2.1 HVL predictions

For monoenergetic x-rays, the half value layer can be derived using basic calculus using the following exponential proportionality:

$$N = N_0 e^{-\mu \cdot x} \tag{3.1}$$

Here *N* is equivalent to the number of particles transmitted by thickness *x* and N_0 is the number of incident particles; μ is a constant of proportionality know as the linear attenuation coefficient. Assuming that the half value layer is the point at which the x-ray beam is attenuated to 50%, one can substitute $N = 0.5N_0$. As a result, the thickness of material (with a particular attenuation coefficient) needed to reduce the x-ray exposure to 50% (x_h) is the following:

$$HVL = x_h = \frac{0.693}{\mu} \tag{3.2}$$

This formula can be applied for a given energy. Knowledge of the interaction coefficient (in m^2/kg) at a particular keV, and the density of the filtering material can be applied to generate the linear attenuation coefficient.

HVL measurements (in mm of Al) predicted for various monoenergetic x-rays (Table 3.1) were calculated using equation 3.2 and attenuation data listed in Johns and Cunningham (1983); the density of Al was taken as $2699 kg/m^3$.

keV	μ/ρ(Al)	μ(Al)	HVL(mmAl)
10	2.6350	7111.87	0.10
15	0.7873	2124.92	0.33
20	0.3375	910.91	0.76
30	0.1101	297.16	2.33
40	0.0557	150.36	4.61
50	0.0363	98.03	7.07

Table 3.1: Linear attenuation of monoenergetic x-rays and comparable half value layers calculated from Johns and Cunningham (1983) data using equation 3.2 and Al density.

A disparity exists in predicting HVL based on the equivalent photon energy (keV) because this value represents the kinetic energy of the x-rays actually exiting the tube. The energy of the x-rays that is set by an x-ray system operator console (given in kV) only characterizes the maximum voltage that crosses the x-ray tube. Thus, electrons leave the LODOX cathode to bombard the tungsten anode create x-rays with energies (in keV) equal to or *less than* the kV.

However, a useful value derived from HVL principles is a back calculation (of Equation 3-2) to generate the energy of x-rays exiting the tube. For example, with a LODOX half value layer of 1.59 mm Al at 40kV (*Table 3.5*), these photons have an average energy between 20 - 30 keV (27.14keV). This prediction can also be verified by HVLs generated in literature (Doi and Chan,1980) (*Table 3.3*) for similar inherent tube filtrations.

Although a spectrum of x-rays varying in keV actually exits the tube, an average value is useful for considering relative beam hardness and the energy imparted to the patient. However, HVLs are more objective than x-ray energy for system comparisons due to spectrum variations. Thus it is essential to use the penetrability of an x-ray beam (in HVL) rather than the kV as a reference point in utilizing conversions (backscatter factors and rad to Roentgen factors) documented by photon equivalent energy (keV) in literature.

3.2.2. Materials and Methods

HVL is dependent upon the energy of the x-rays. As a result, a single x-ray generator maintains a number of HVLs. For mammographic measuring purposes, LODOX will be used at lower kVp and hence HVL must be calculated at the lowest possible energy of the tube (40 kV). The accepted method for measuring HVL (Johns and Cummings, 1983) requires varying the aluminium filtration thickness of an x-ray beam until the resultant exposure has been reduced by 50% of its original unfiltered value. The set-up requires that the filtration normally present during an x-ray remain undisturbed while the additional filtration is added. The tube and housing used in the LODOX-PPM machine (Comet AG, type DBX-200-270-2022H) has a combined inherent filtration of 1.7 mm of Al. The aluminium mirror that is present in the x-ray generator creates a total scan filtration of 2mm when it is placed at an angle of 45 degrees.

Universal Unidos Dosemeter (Model 10002; Serial number 20001) was attached to a 0.02cc Ionization Chamber (Model W 23342; Serial number 948). Both were manufactured by PTW (Freiburg). These instruments have been calibrated against the National Standard RD-01, corrected to 20 degrees Celsius and 101.3 kPa and issued on 06 March 2001. According to calibration certification the uncertainty does not to exceed $\pm$ 2%. Filters from a Gammex Aluminum Half Value Layer Attenuator Set are used to decrease the x-ray exposure, held by a standard scientific stand with a three-pronged clamp. The filters are positioned 50cm above the detector to avoid radiation scattered from the aluminum, and over 50cm from the source. Likewise, there are no scattering agents within 50 cm of the testing apparatus. The ionization chamber is placed in the center of the x-ray beam to maximize the intensity of the dose, as recommended in the literature (Johns and Cunningham, 1983).

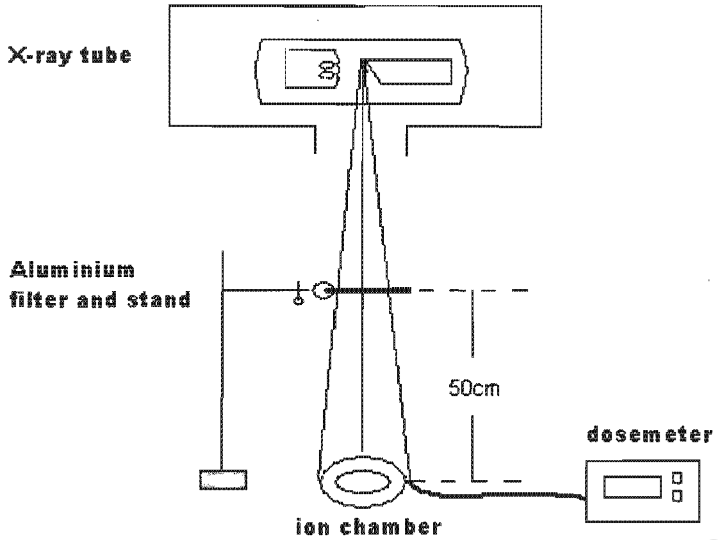

Figure 3.1: Experimental setup used to measure LODOX HVL. Ionization chamber was placed in the direct center of the beam and objects which may contribute to scatter were a minimum of 50cm away.

Readings are acquired from the dosemeter in pC at filter variations from 0 – 5.0mm of aluminium using incremental improvements of 0.5mm Al. Exposure measurements were taken at various x-ray energies (kVs) and intensities (mA). LODOX exposure lasts for 1000ms and the dose is integrated over a period of 15s to account for the startup time of the x-ray generator and insure complete absorption. The HVL is the point at which the exposure is equal to half its original, unfiltered value. These values were derived using best-fit treadlines and are listed in the results section (Table 3.2).

Additionally, preliminary beam testing was performed using standard radiographic films and a KODAK X-Omat V therapy verification pack (See Appendix A). Beam testing was done for two purposes: firstly, to observe and compare beam uniformity; and secondly, to determine the width of the LODOX beam at the level of the detector. It was important that the ionization chamber was completely covered by the beam for consistent exposure recordings. This is because the ionization chamber may accidently be moved during filter changing, allowing a variant portion of the chamber to collect charge during x-ray exposure. To insure adequate coverage with such a small beam width, preliminary beam width measurements illustrated the importance of a directly centered chamber. (A film at the detector illustrated a width of 0.55 - 0.60 mm while the chamber diameter according to specifications is 0.52mm.)

3.2.3 Results

Energy	Intensity	HVL
(kV)	*(mA)*	*(mm Al)*
40	80	1.59
40	100	1.54
40	125	1.64
70	80	2.85
70	125	2.77
100	80	4.17
100	125	4.04

Table 3.2: Measured LODOX Half Value Layers generated at various intensities determine precision.

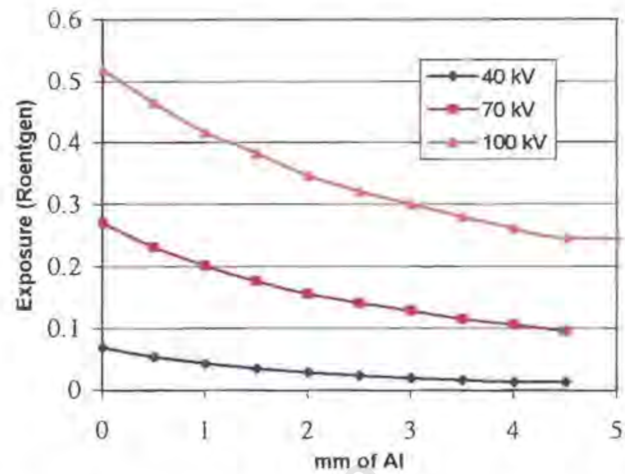

Figure 3.2: Comparison of aluminium filtration at varying kV. Higher energy x-rays exhibit larger HVLs (higher x-ray penetrability).

UNIDOS measurements were initially recorded in pC. Absorbed dose readings, in Gray (J/kg), were calculated using both conversion (1.050E09Gy/C) and calibration factors (0.931 Air Kerma Gy / Displayed Gy) documented by the Certificate of Calibration. Since HVL measurements are calculated based on exposure (in Roentgen), the absorbed dose values were then converted using standardized factors: 1 R = 87.33 J/kg air (Johns and Cummings, 1983). This set of calculations resulted in exposure measurements (in Roentgen), at each 0.5 mm of Al filtration, as seen in Figure 3.2. Since the HVL is literally the point at which the exposure is decreased by 50%, the unfiltered dose was divided by 2 and the subsequent equivalent filter value was equated using best line fit plots. Second order polynomial trendlines generated the best fits with R^2 values ranging between 0.985 and 1. The resulting HVLs are given in Table 3.2.

The exposure taken at each 0.5mm filtration of Al is illustrated in Figures 3.2 and 3.3. The exposure response at given filtrations is nonlinear because the charge captured by the ion chamber and recorded by the detector is not monoenergetic. As each filter layer is added, the actual quality of the beam changes. With increased filtration, the energy of the transmitted x-rays becomes more monochromatic. Although the purpose of filtration is to remove excess radiation that will be absorbed by the body (primarily lower kV x-rays), mammography uses lower energy x-rays than other forms of diagnostic x-ray imaging. As a result, less filtration is required for breast imaging because the photons that are normally filtered out are useful for mammography.

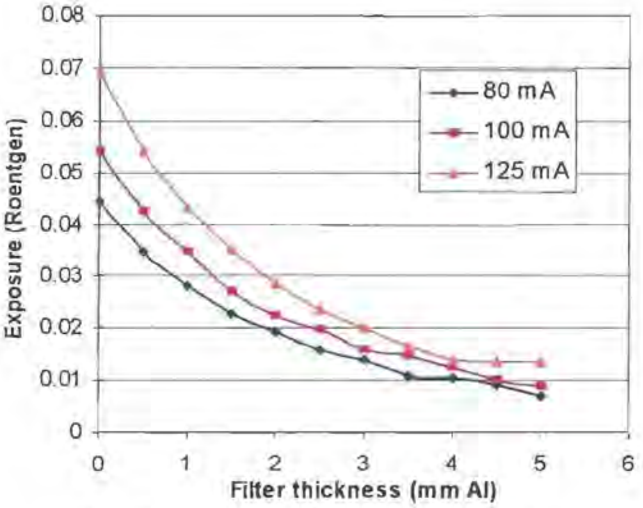

Figure 3.3: Comparison of aluminium filtering at various x-ray intesities (40kV). X-ray intensity slightly increases the exposure but does not significantly alter the HVL.

Half value layers increase with x-ray energy because the penetrability of the beam is greater at higher energies. X-ray penetrability varies for different systems because it is dependent upon the components that create the x-ray spectrum. The lowest setting on LODOX is 40kV, hence HVL was measured at this setting for the purposes of quantifying mammography feasibility. Mammograms are usually taken between 24-32 kV but it was not possible to recreate these kVs on the LODOX machine. For the purpose of generating a good range of data, additional HVLs were recorded at both 70 and 100kV.

Typical mammography tube currents range from 80-100mA (Huda and Slone, 1995). Exposure measurements were taken at both 80 and 125 over the range of kV values (40,70,100kV) to measure precision. Measurements were taken at 125 mA because this value, when multiplied by exposure time, in this case 1000ms, is comparable to mammographic intensity exposures for 3 – 4 cm breasts in milliamp seconds (125 mAs).

As expected, the half value layers for the graph above (at 40 kV) differ very slightly and show no direct variance with mAs. For example, the highest recorded HVL (1.64 mm Al) was recorded at 100kV while the lowest (1.54 mm Al) was recorded at a higher x-ray energy, 125kV. This variation may be due to experimental setup. The resulting HVL values for the same kV (at varying mAs) show standard deviations of ± 0.04, ± 0.04, and ± 0.07 mm of Al for 40, 70, and 100 kV, respectively.

3.2.4 Discussion

The LODOX-MP is capable of an x-ray energy range (40-153kVp) much higher than what is required for mammography (~24-32kV). Thus, calculating the HVL at 40 kVp is the closest measurement achievable to mammographic voltages for this study. Hammerstein, *et al.* (1979) calculated the HVL using tungsten/aluminum and molybdenum target/filter combinations. These measurements provide a valuable reference for comparison with LODOX-MP measured HVL values for soft x-rays. It is noted that the listed LODOX value is the average of HVLs generated at 80, 100, and 125 mAs to characterize the current of typical mammographic x-ray tubes.

Author	**Anode**	**Energy**	**HVL (mm Al)**
Doi and Chan (1980)	W	25.4 keV	1.50
	W	28.5 keV	2.00
	W	43.0 kV	1.22
Hammerstein *et al.* (1979)	W	40.0 kV	0.79
	W	50.0 kV	1.21
LODOX-MP	W	40.0 kV	1.57

Table 3.3: Comparison of literature HVLs. LODOX beam energy exiting the tube cannot be quantified precisely in keV but is equivalent to monoenergetic x-rays between 20-30keV (*3.2.1*).

From this assessment, it is evident that a LODOX x-ray beam exhibits higher penetrability (harder x-rays) than mammographic systems, even at low energy (40kV). This should be expected because LODOX was not created as a mammographic machine. Hard x-rays are more constructive for regular diagnostic radiography. However, in order to create a LODOX-based dedicated mammography system, less penetrability is required due to the slight density differences in composed breast tissue. As a result, a lower amount of inherent filtering, and the varying concentration of x-rays (due to the Heel effect) will have to be taken into account in designing such a device.

Target/Filter	Inherent Filter	Energy	First HVL
	(mm Al)	*(kV)*	*(mm Al)*
W/Al	1.78	50	1.21
W/Al	1.27	40	0.79
W/Al	0.64	30	0.36
Mo/Mo	0.03	28	0.31

Table 3.4: Mammography HVL values from Hammerstein *et al.* (1979).

Target/Filter	Inherent Filter	Energy	First HVL
	(mm Al)	*(kV)*	*(mm Al)*
W/Al	2.00	100	4.11
W/Al	2.00	70	2.81
W/Al	2.00	40	1.59

Table 3.5: LODOX HVL values illustrate the hardness of LODOX beam in comparison to other

One explanation for higher LODOX half value layers at comparable energies lies in the inherent filtration of the x-ray system. The target/filter combination, and particularly the amount of inbuilt filtration in the x-ray tube, alters the amount of filtration required to reduce the initial expose by a half. The inherent filter thickness of the LODOX-PPM machine, as stated previously, is 1.70 mm of Al angled at 45 degrees. However, since the filter is angled, it achieves a total filtration of 2.0 mm of Al, rather than 1.70. As a result, the HVL measured for LODOX is higher than literature values at comparable energies (Table 3.4) because the thicker filter allows less low energy radiation to pass and hence the penetrability of the beam is greater.

International standards for inherent filtration in mammography (soft x-rays energies) are a great deal lower than for other types of radiography. For example, while diagnostic machines used in routine examinations require at least 3.0 mm of Al permanently filtering the x-ray output, a total filter of 1.5 mm of Al is required for xeroradiography (40-50kV) (Johns and Cunningham, 1983). For mammograms taken at approximately 30kV a total filter less than 1.0 mm of Al is usually inherent to the system. The HVLs listed by Hammerstein *et al.* (1979) with 1.78 mm Al filtration generated a first HVL of 1.21 mm Al at 50kVp. This is the closest mammography-specific value (comparable to LODOX HVL) found in the literature.

Aside from inherent filtration, systemic filtering also exists in the form of the window through which the x-ray beam passes out of the tube housing. For body imaging such as LODOX, x-ray tube windows are composed of glass, which absorbs many of the unwanted low energy photons. Unfortunately, these photons are the useful beam component for breast imaging. As a result, beryllium is used instead of glass for dedicated mammography units to reduce the amount of window filtration.

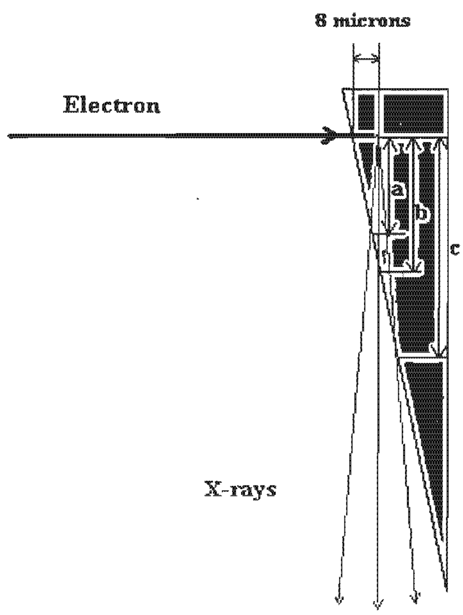

Figure 3.4: X-ray production occurs ~8 microns inside the target. Differing exit lengths result in decreased radiation for x-rays with a longer path (on the anode side).

An additional explanation for higher LODOX HVL involves the concentration of beam intensity. The purpose of angulation in diagnostic tubes is to increase the heat loading capacity of the anode. Both kilovolt and ampere increases add to the heat distributed to the entire anode, which degrades tube performance. Angulation concentrates a larger stream of electrons onto a smaller focal spot, without directing superfluous heat to one particular point on the target. As a result, better resolution is allowable without excess anode damage. Some systems, including LODOX, use rotating anodes for additional heat dissipation.

The Heel Effect describes the varied intensity of x-rays that results from the angulation of the anode target. When electrons strike the anode, the actual x-rays are not produced on the surface but 8 microns *inside* the target material itself (Andolina *et al.*, 1992). X-rays on the anode side are less intense because they travel a longer distance through the anode (as seen in Figure 3.3). These x-rays are more likely to be reabsorbed by the anode itself than those with a shorter distance through the target material. As a result, steeper target angles create a more pronounced Heel Effect.

In mammography tubes, x-rays from the stronger radiation side (the cathode side) are directed at the chest wall, while the weaker radiation (the anode side) is aimed towards the nipple. Other diagnostic x-ray tubes exhibit the heel effect in a pattern that differs by 90 degrees, where photon intensity is distributed in a left-to-right pattern. The anode angle used for mammographic x-ray tubes is usually between 6 and 16 degrees from the perpendicular of the detector. Since the anode angle for LODOX technology (a Varian tube) is 7 degrees, tube angle does not appear to be a major factor in Heel Effect differences.

The magnitude of the Heel Effect is also dependent upon factors such as the field size, and SID (Huda and Slone, 1995). The SID influences the Heel Effect because as the tube is distanced from the detector, the intensity of the x-rays varies inversely as the square of the distance. Thus, a larger SID, such as that of the LODOX-MP, will exhibit much less of a Heel Effect. LODOX utilizes a scanning line beam, which is a great deal smaller in field size than a typical mammography cone beam. The LODOX-MP x-ray beam is recorded as 3 mm in width at the detector. If a breast 16cm in diameter were imaged by both LODOX and a dedicated mammography unit, the field size would differ by a factor of 50 (approximately 250cm^2 versus 5cm^2 for a LODOX image). This decrease in field size results in a less significant Heel Effect because the intensity of the beam varies much less over the 3 mm width of the line beam than over the entirety of a 16cm cone width.

Exposure	Film density			
AEC	3.64	3.63	3.63	3.63
AEC	3.67	3.68	3.65	3.64
AEC	3.70	3.69	3.66	3.66
AEC	3.70	3.71	3.69	3.71

Table 3.6: A film taken at 35 kV on a standard screen-film mammography system with automatic exposure control (AEC). The Heel Effect is apparent from the regular increase in film density in the vertical direction. The breast is normally placed at the side with the highest intensity.

To analyze this conclusion, densitometer readings of LODOX films and mammography films taken by a standard screen-film system (GE Senographe 600T) and compared to LODOX beam uniformity (see Appendix A). As predicted, the film density, and hence the beam density, increases in the direction of the chest wall for the screen film image. In contrast, the narrow beams of LODOX retain a relatively uniform density at each exposure time, primarily because the field size is significantly smaller.

According to the National Council on Radiation Protection and Measurements (Feig, *et al.*, 1986), the optimal HVL for screen-film mammography systems is 0.3 to 0.4 mm of aluminum. The typical x-ray tube energy used in standard mammography (approximately 20-36 kV) is lower than the softest x-rays generated by the LODOX-MP

(40 kV), which contributes to LODOX's higher HVL measurement. From graphs above it is obvious that larger kV values generated higher HVL measurements due to their inherently higher energy. It was also noted that changes in the intensity of the x-rays did not have a significant effect on the half value layer. However, discrepancies in energy do not entirely account for such high penetrability. As discussed, increased filtration and the Heel Effect also influence LODOX beam quality.

3.3 Contrast

In digital mammography, the stored image reflects the subject contrast, devoid of receptor contrast, because its signal is directly (or logarithmically) proportional to the amount of radiation transmitted through the breast. The recorded intensities can be transformed into optical density on a laser-printed film or it corresponds to the brightness on a monitor. On a monitor contrast is alterable so that the image can be presented in a variety of ways.

3.3.1 Theory

To measure the contrast ratio (CR), intensity of a region and its direct surroundings must be measured:

$$CR = abs\left(\frac{I_1 - I_2}{I_1 + I_2}\right) \tag{3.3}$$

The CR is also dependent upon the thickness and density of the object. As a result, derivations of this equation with respect to material density and thickness can be used to determine the CR of an imaging system. Using the signal levels (S_a and S_b) over the area of two blocks, contrast is defined as the following:

$$\text{Contrast} = \frac{S_a - S_b}{S_a + S_b} \tag{3.4}$$

With LODOX technology, dark current subtraction, flat field normalization, and logarithmic conversion are applied to the data signals. The individual signals can be translated into a function of their intensity with the equations listed in Appendix B

(Booysen, 1998). By substituting density factors and equating the flat field intensity to the intensity at height z_2 above the detector, contrast can be reduced with the following derivation:

$$\text{Contrast} = \frac{z_1\mu_1 - z_2\mu_2}{z_1\mu_1 + z_2\mu_2} \qquad (3.5)$$

Therefore, if the blocks have the same thickness, than the blocks can be expressed solely in terms of density. Likewise, if the blocks have similar densities, the thickness may be used to determine the image contrast.

$$\text{Contrast} = \frac{z_1 - z_2}{z_1 + z_2} \qquad (3.6)$$

$$\text{Contrast} = \frac{\rho_1 - \rho_2}{\rho_1 + \rho_2} \qquad (3.7)$$

Thus, by using two blocks differing in either thickness or density, one may measure image contrast. This also illustrates the dependence of imaging contrast on thickness and density (of breast tissue) for diagnostic and detection purposes. In mammography, the thickness of the breast should be relatively uniform if compression is being used. The density of the breast is variable however, and consists primarily of glandular and adipose tissue.

3.3.2 Materials and Method

The test tools used for this section, the PTW NORMI 58, employ variations in thickness of aluminum and copper to quantify contrast as a percent. The amount of measurable contrast ranges from 0.8%-5.6% for the NORMI 58. Using adjustable contrast through the user interface, contrast is available up to the smallest reading, 0.8%. Most importantly, the ability to adjust contrast results from a linear relationship between signal intensity and exposure. In comparison, high contrast in screen-film systems occurs within a much smaller range of exposure latitude (as seen in Chapter 2).

3.3.3 Results and Discussion

The contrast capabilities of digital imaging exceed the ability of screen-film systems. The narrow latitude of a high contrast region in screen-film mammography, for example, limits the differentiation of objects with similar densities. The contrast and brightness of digital systems can be manipulated in the soft copy display. This facilitates and personalizes reading x-rays from a monitor, as opposed to a visually inflexible back-lighting system.

LODOX utilizes 16,000 grey scale levels for gray-level transformation. Using contrast stretching, a range of gray-levels of information can be selected. This enhances the image because the selected range is mapped to the full scale display of gray-levels, thus being "stretched" to cover the new visible range. The range that is selected can be adjusted to include and position or width of the original grey-scale.

3.4 Scattered Radiation

Scattered x-rays that are recorded by a detector (after passing through the breast) lessen image contrast. Scatter also lowers the high spatial frequency content of an image by degrading border sharpness. To quantify these effects, the scatter to primary ratio (SPR) compares the amount of scattered radiation recorded with the directly transmitted x-ray intensity. Also used to quantify scatter is the scatter fraction (SF):

$$\mathrm{SPR} = \frac{\mathrm{S}}{\mathrm{P}} \tag{3.8}$$

$$\mathrm{SF} = \frac{\mathrm{S}}{\mathrm{S}+\mathrm{P}} \tag{3.9}$$

The relative intensity of scattered radiation is essentially independent of kVp, but varies with phantom (breast) thickness and radiated field size (Barnes and Brezovich, 1978). Harder incident beams create a broader spatial distribution of the scattered radiation. Quantification of noise can also be calculated as a signal to noise ratio (SNR) (see Appendix Noise). Likewise, Doi and Chan (1980) use Monte Carlo simulated backscatter factors (BSFs) describe the amount of scatter that occurs in the breast in order to determine the radiation dose delivered.

3.4.1 Methods and Materials

Scattered radiation conditions in the mammography setting can be simulated using the Monte Carlo technique (Boone, 2000). A convolution method using ideal mammogram geometry can be applied to produce scatter point spread functions (PSF), which can then be used to calculate approximate SPR values. With this method, SPR can be calculated as a function of breast thickness and size, taking into account the x-ray spectrum, breast thickness and composition, field of view, air gap, and the position of interest:

$$SPR = \left[a + b \times (d)^{1.5} + c \times (z)^{-0.5}\right]^{-1} \quad (3.10)$$

For the equation above *d* is equal to diameter of the (semicircular) breast in centimeters, *z* describes the thickness of the breast in centimeters, and *a*, *b*, and *c* are coefficients determined by Monte Carlo simulations (*a* = -2.335, *b* = 22.396, and *c* = 8.851). This equation produces SPR data for breasts up to 8cm in thickness and from 3 to 30cm in diameter with an average error of only 1%.

3.4.2 Results

Although the amount of scatter imaged in mammography is independent of the beam quality, it varies with breast size and thickness. For 3-6cm breast phantoms, Barnes and Brezovich (1978) measured SPR values between 0.4-0.8. Using Equation 3-10, SPR values for an average breast (d = 10-14 cm, z = 3-6 cm) have been calculated in the table on the right.

thickness (cm)	diameter (cm)	SPR
3	10	0.29
3	12	0.30
3	14	0.31
4	10	0.36
4	12	0.38
4	14	0.40
5	10	0.43
5	12	0.47
5	14	0.49
6	10	0.51
6	12	0.56
6	14	0.59

Table 3.7: Various SPR Values for breast diameters and thicknesses using Equation 1-10 (Boone and Cooper, 2000)

For a breast with a thickness of 4 cm and a diameter of 14 cm, the predicted scatter to primary ratio of a conventional mammography machine would equate to 0.40. Thus the amount of scatter in a LODOX scan is lower than the scatter in normal mammographic systems. Low amounts of scatter result in better contrast, as well as a higher signal to noise ratio. Similarly, for low SPR smaller amounts of radiation are required for a particular signal to noise ratio.

Additionally, Boone *et al.* (2000), computed scatter reduction factors (ratio of SPRs) for 2mm, 10mm, and 12mm slot widths of slot scanning mammography systems. Using the reduction factor for a 2mm width beam (the closest approximation to the LODOX beam), the predicted scatter reduction factor from Boone is 11.7 for a breast thickness of 4cm and diameter of 15cm. Thus, the scatter to primary ratio calculated using Boone's algorithm and scatter reduction factor for a scanning system (breast thickness = 4cm, diameter = 15cm) is 0.06, a much lower value than predicted for non-scanning mammography systems.

3.4.3 Discussion

The published SPR for LODOX technology is 0.2, which compares exceptionally well with a conventional x-ray signal to primary ratio of 8.72 (Booysen, 1998). In accordance with the literature (Barnes and Brezovich, 1978 and Boone *et al.*, 2000), the reduction in detector size reduces the amount of exposure to scattered x-rays, resulting in higher contrast. Consequently, a higher signal to noise ratio (SNR) also occurs.

In mammography, SPR is dependent upon both field of view (FOV) and breast thickness (Barnes and Brezovich, 1978). The primary function of compression is to decrease breast thickness in an effort to lower SPR. The LODOX scanning technique introduces a small area for the FOV (and hence a smaller SPR). As a result, the thickness allowable for adequately imaging a breast could potentially be larger. The LODOX SPR (0.2) is lower than the predicted value for standard mammography systems for a breast thickness of 4cm and a diameter of 14cm (SPR=0.40), suggesting that less scatter is comparatively evident. However, compared to the predicted SPR of a scanning mammography system (0.06 for 4cm thickness and 15cm diameter), LODOX does not perform as well.

3.5 Spatial Resolution – Modulation Transfer Function

Spatial resolution expresses an imaging system's ability to record fine detail. This parameter can be compromised by blurring, which can result from patient motion, x-ray intensity distribution (geometric blurring), or receptor blurring. By imaging a pattern with equally spaced x-ray opaque bars, one can ascertain a measure of limiting spatial resolution (LSR). Using 100% contrast, the greatest number of bars and spaces (line pairs) per mm that can be resolved determines the ability of the system to record fine spatial detail. Screen-film mammography systems usual measure at around 10 lp/mm and higher however. The FDA guidelines for screen film mammography equipment requires that each machine "shall provide a minimum resolution of 11 lp/mm when a high contrast resolution bar test pattern in oriented with the bars perpendicular to the anode-cathode axis, and a minimum resolution of 13 lp/mm when the bars are parallel to that axis."

In general, LSR values of digital systems are lower than their screen-film counterparts. Due to the contrast capabilities of digital systems, smaller LSR values are necessary to create quality images. The Modulation Transfer Function (MTF) quantifies the transmission degradation of every component of an imaging system (tube parameters, detector, *etc.*) on the final image quality. Unlike measurements of limiting spatial resolution (lp/mm), MTF measures the ability of an imaging system to actually transfer the modulation (contrast) to a final recorded image. Thus, it can be used to describe the contrast limitations of an imaging system. For example, an MTF of 0.5 would demonstrate that the inherent contrast of the original object decreases by 50% in the recorded image. Additionally, MTF measurements are understood to also relay the resolution properties of an imaging system (Samei *et al.*, 1998).

According to Haus and Yaffe (2000), MTF describes the relationship between contrast and resolution in imaging patterns whose x-ray transmission varies sinusoidally with position. Conveyance of radiological imaging patterns can thus be described as an array of sinusoidal waves with variant amplitudes and spatial frequencies. High frequencies correspond to fine detail while lesser frequencies imply rougher image resolution.

To measure the MTF of an imaging system, one must input a signal, and analyze the resultant output. The output image g(x,y), assumed to be a linear transfer function, is produced through convolution with an operator h(x,y) that is independent of position.

$$f(x,y) \rightarrow \boxed{h(x,y)} \rightarrow g(x,y) \qquad (3.11)$$

The input symbol is assumed to be the sinusoidal variation of x-ray fluence (the number of x-rays per area). The frequency of this signal, also referred to as *spatial frequency*, is the reciprocal of the distance between the peaks of the sine waves. The output signal will also be sinusoidal but changes in frequency by the factor 1/M, where M is the magnification of the imaging system (Johns and Cunningham, 1983).

The Fourier transform of h(x,y) is the Optical Transfer Function (OTF) of the system. The calculated magnitude of the OTF is the MTF. While the OTF illustrates the transfer of intensity modulation at variant frequencies throughout the system, the MTF determines the attenuation of these signals. Given a function that describes the distribution of a radiation pattern along an x-axis, the following function describes its Fourier transform:

$$H(f) = \int_{-\infty}^{+\infty} \varphi(x) e^{-2\pi i f} dx = \int_{-\infty}^{+\infty} \varphi(x)(\cos 2\pi fx - i\sin 2\pi \sin 2x \qquad (3.12)$$

H(f) is the Fourier transform of h(x), f is the spatial frequency, and i is the square root of –1. Additional information of Fourier transformation is given in Appendix B.

3.5.1 Methods and Materials

A common method of calculating MTF involves measuring the line spread function (LSF) of a system using a narrow slit a few tens of microns wide (Morishita *et al.*, 1995; Johns and Cunningham, 1983). The MTF is then calculated from the signal generated from the observed pattern of x-rays using Fourier transformation.

An alternative technique involves measuring the Edge Spread Function (ESF) or Edge Response Function (ERF) of a uniformly thick opaque plate with a straight edge (Samei and Flynn, 1998; Gransfors and Aufrichtig, 2000). To calculate MTF the ESF is differentiated (to create the LSF) and then a Fast Fourier Transformation (FFT) is implemented.

$$MTF = |FFT(LSF)| = |FFT(ESF_{k+1} - ESF_k)| \tag{3.13}$$

The FFT serves to amplify all signals proportional to the signal frequency. Calculating a one-dimensional Fourier transform of the derived LSF results in the Optical Transfer Function (OTF) of the system, which represents the frequency content of the image response (Booysen, 1998). Using a two–dimensional Fourier transform results in the MTF. To measure MTF accurately the plate edge should be as sharp as possible and the OTF should have an impulse close to one, which indicates perfect signal transmission.

In digital systems, variations in receptor sensitivity creates a fixed pattern of noise. As a result *flat fielding*, recording the image of a uniform field of x-rays as a correction control, is used to subtract fixed digital noise. To do this the imaged signal and the flat field signal are both divided by the maximum flatfield signal, and a ratio of the resultant values create the graphical representation of the ESF (seen in Results). Thus, MTF is mathematically defined as the magnitude of the Fourier transformation of the LSF, divided by the magnitude at zero frequency (Gransfors and Aufrichtig, 2000). The resulting MTF curve is analyzed versus spatial frequency (v) where (v_0/v) is an integer and v_0 is equivalent to the Nyquist frequency. For the LODOX-MP, the Nyquist (1/2p) is 8.33 cycles/mm due to the 60micron pixel width (p). Edge image acquisition was used for calculating the MTF for this study. The ESF was generated using a tungsten plate, which was isolated on the interface operator to 512 pixels (corresponding to 512 sampling points).

3.5.2 Results

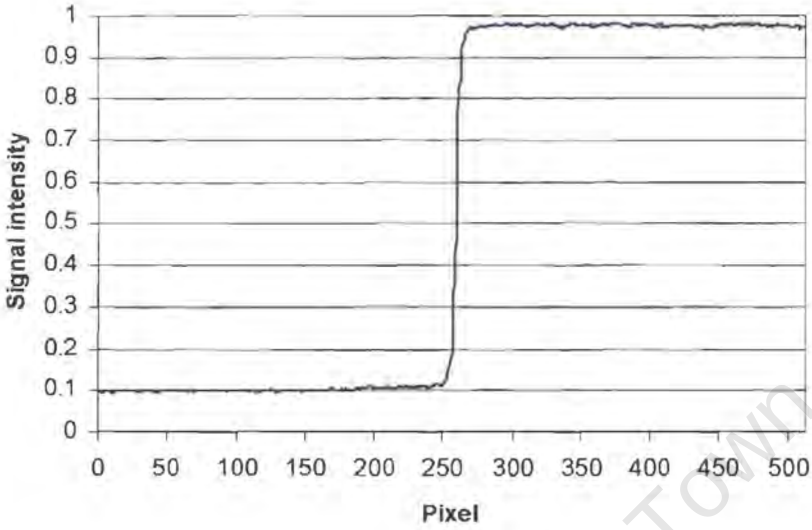

Figure 3.5: Edge Spread Function (ESF) of a tungsten plate generated by the LODOX-MP over a range of 512 sampling points.

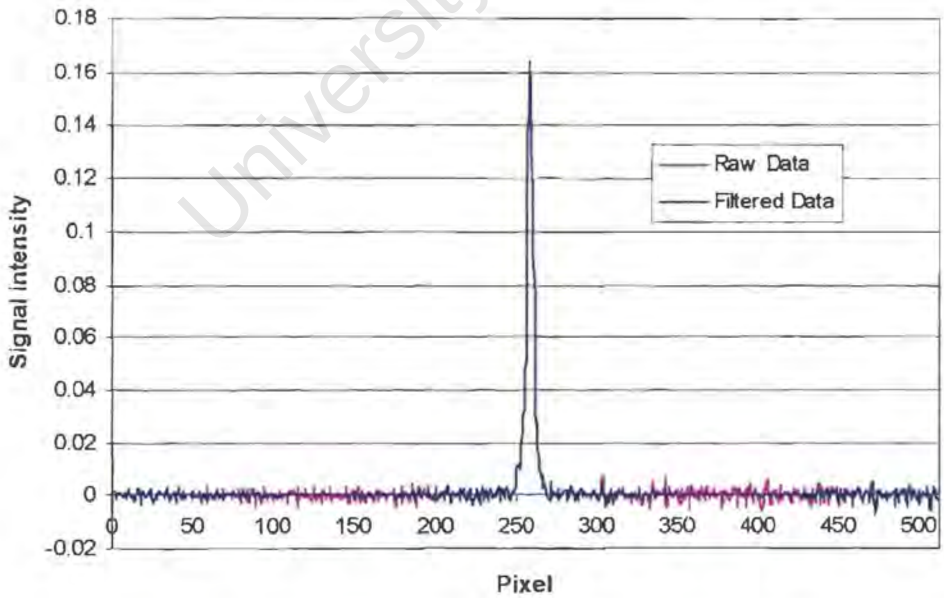

Figure 3.6: Line Spread Function (LSF) calculated by the differentiation of the LODOX ESF. A Hanning filter (Samei *et al.*, 1998) was applied to the LSF to reduce noise unassociated with the edge transition.

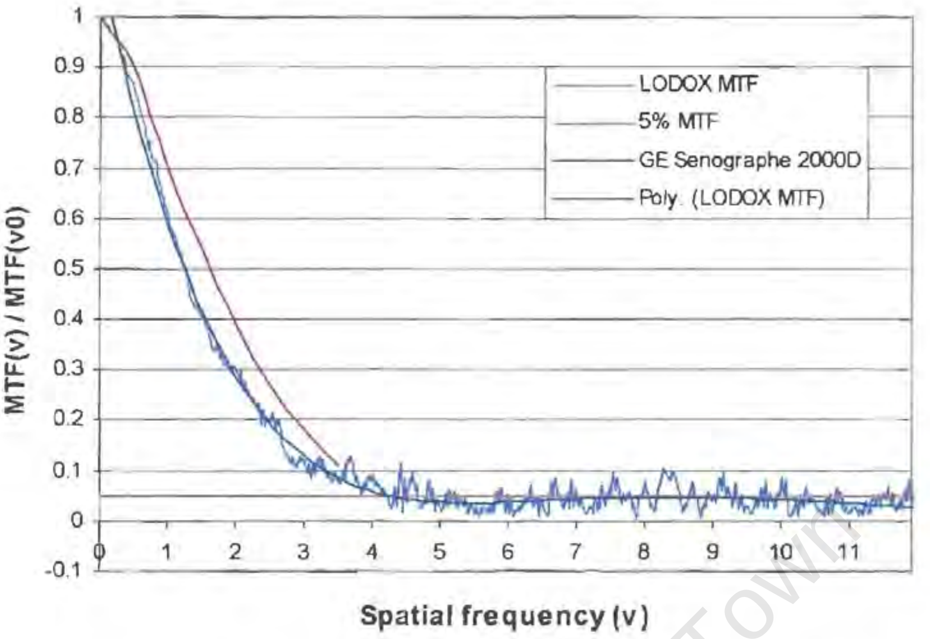

Figure 3.7: Modulation transfer function (MTF) results from a Fourier transformation of the LSF. A best fit LODOX MTF is compared to data from the GE Senographe 2000D. Digital mammography systems should be capable of 5% MTF at 8-10 cycles/mm (Williams *et al.*, 1997).

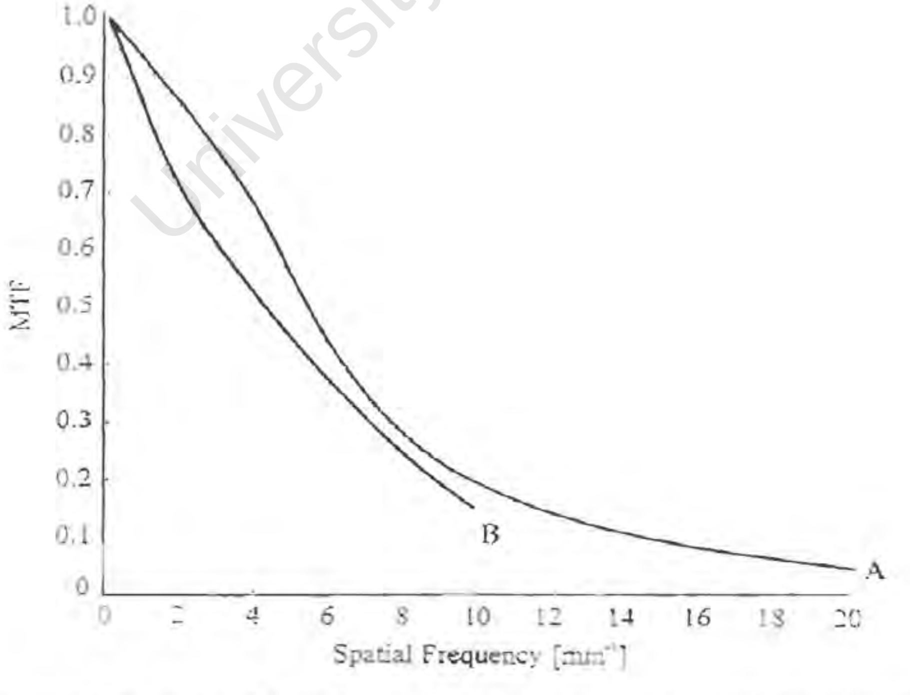

Figure 3.8: MTFs of typical screen film mammography receptor (A) and digital receptor with 50 micron detector elements (B). Graph taken from Haus and Yaffe (2000).

3.5.3 Discussion

Total systemic MTF of the LODOX-PPM is illustrated in Figure 3.7. A Hanning filter was used to filter the LSF signal (as done in Samei *et al.*, 1998) and a fifth order polynomial was fit to LODOX MTF data for comparison.

An illustration of generic MTFs (Figure 3.8) illustrates that digital detectors have the potential for better MTFs at higher spatial frequencies. However, factors other than the detector also degrade the total MTF. LODOX MTF, in comparison to the general graph, exhibits much greater noise than the general representations of detector MTF.

The average LODOX MTF values at various spatial frequencies are lower than the MTF values measured by Gransfors and Aufrichtig (2000) for the GE Senographe 2000D. At 0.5, 1.0, 1.5, 2.0, and 2.5 cycles per millimitre LODOX MTF values were 0.82, 0.57, 0.38, 0.27, and 0.20, respectively, compared to GE Senographe 2000D values of 0.89, 0.71, 0.53, 0.37, and 0.26 for the same spatial frequencies. Detector design goals for digital mammography systems with a pixel size of 50–75 microns, yield limiting resolutions of 7–10 cycles per millimetre. For this pixel size to be useful, the modulation transfer function (MTF) should be greater than 5%–10% out to 8–10 cycles per millimetre (Williams et al, 1997). LODOX conforms to the lower end of this parameter with an average MTF of 5.02% between spatial frequencies of 8-10 cycles/mm.

Limiting spatial resolution has also been expressed in terms of the frequency at which the MTF equals 4-5% (Rossman, 1963). Although this relationship is not precise (Haus and Yaffe, 2000), it offers another means of measuring the experimental lp/mm of a system. For the LODOX-MP, the limiting spatial resolution at 5% MTF is measured as 4.16 lp/mm. Using a

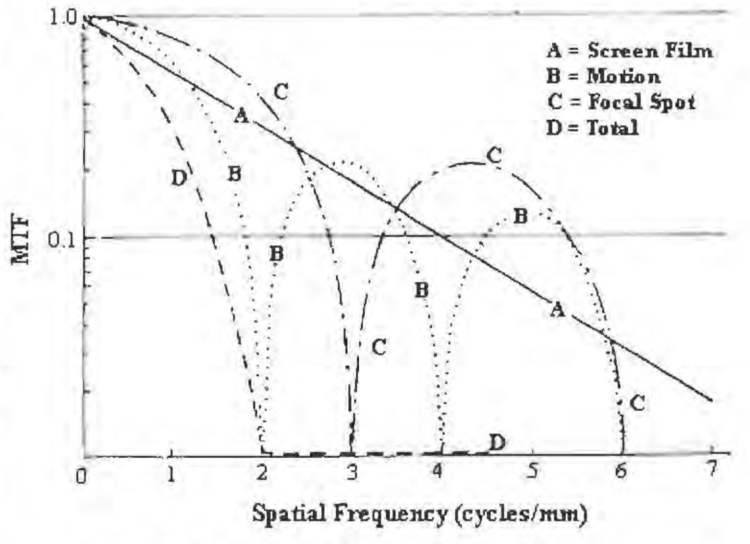

Figure 3.9: Illustration of the diverse contributing MTF factors to the total measured MTF. Adapted from Johns and Cunningham (1983).

lp/mm test tool at the 1 pixel binning mode (the test mode used to measure MTF), the limiting spatial resolution was measured at approximately 4.25 lp/mm. Potentially, the LODOX detector has the capability of imaging up to 8.3 lp/mm (as stated by LODOX published data) however, other degradation factors of MTF, such as motion and the focal spot, also limit the system. A logarithmic graph emphasizes various systemic contributions to MTF (Figure 3.9).

Compared to the only digital mammography unit on the commercial market (GE's Senographe 2000D), LODOX is less capable of transferring contrast. Shortcomings in LODOX MTF in comparison to mammographic specific systems stem from the fact that the LODOX-PPM was designed as a full body scanner rather than a dedicated mammography unit. Since mammography requires intensified resolution capabilities, parameters of the system that affect MTF are not particular to mammography. As a result, the sensitivity of the LODOX system components (x-ray tube parameters, SID, etc.) do not conform to mammographic standards. However, the graphical proximity of LODOX MTF to an FDA-approved system (Figure 3.7) suggests that this type of technology may be suitable for a mammographic prototype with certain modifications (Chapter 5).

Despite precision in placement, slight angulation of the test target edge may have led to a less optimal MTF. Unlike measuring MTF in screen-film x-ray systems, the coarseness of the display matrix in digital systems complicates the response function. Presenting an image in pixels as a particular intensity of grey makes it difficult to obtain an adequate sampled response. By angling the input slightly, relative to the columns of the display matrix, and merging several rows of data (each slightly shifted), one can obtain a sufficiently sampled response (Sones, 1984). Angling can also introduce methodical error because in order to determine the exact perpendicular distance from each pixel to the test device, the exact position and angle of the test device must be known (Samei et *al.*, 1998). Thus, the placement of the target along with aliasing, are possible sources of experimental error.

3.6 Detected Quantum Efficiency

Detected quantum efficiency (DQE) has been accepted by industry as the most important parameter of radiographic diagnosis, because it associates the effects of both noise and contrast, and allows for comparison of imaging systems with different technological designs. DQE can be used to determine how much degradation (of SNR) occurs in the detection stage of an imaging system before it is processed or displayed. DQE is usually expressed as a function of object detail or spatial frequency.

DQE, a measure of efficiency, represents a ratio of the noise equivalent quanta (NEQ) at the final image to the NEQ at the entrance of the detector.

$$DQE = \frac{NEQ_{out}}{NEQ_{in}} = \frac{SNR_{out}^2}{SNR_{in}^2} \tag{3.14}$$

The higher the SNR, or NEQ, the easier it is to distinguish an object from background noise (Haus and Yaffe, 2000), and using a ratio allows for an efficiency rating due to quantum effect. Higher DQE implies that the probability of detecting incoming photons is greater. Thus, a system with a high DQE could utilize a greater proportion of the incident photons and at the same time create the minimum amount of additional noise. For example, for an ideal system capable of recording every incident photon, DQE would measure to 100%. However, a high DQE does not necessitate a valid image (for example, if too few photons are used to create the image).

As noted, the output SNR is a relative measure of image quality, and the input SNR is proportional to patient dose. Subsequently, DQE results in the quantification of an image quality to radiation comparison. This is useful in determining how doses vary with image optimization because a detector with a high DQE suggests that image quality can be improved without unnecessary patient irradiation. Unlike limiting spatial resolution measurements, detected quantum efficiency (DQE) combines the performance of both noise and contrast. Low noise and high contrast are equally crucial to produce a high-quality image. If a noisy system (low SNR) exhibits high contrast, its image will appear speckled and erratic (by quantum interferences) and thus unreadable. Likewise, a system with a high SNR but low contrast will yield images that lack differentiation.

Although DQE measurements are quoted in industry, no standardization of this measurement currently exists. The International Electrotechnical Commission (IEC) will publish Working Group 33 – "Characteristics of digital X-ray imaging devices – Determination of the detective quantum efficiency" by the spring of 2002 (Hannon, 2000). A committee draft of this document was procured with the intent to model DQE measurement as advised by the IEC (IEC, 62B/416/CD, 2000). However, the scope of this model "is not applicable to digital detector systems intended to be used in mammography, dental radiography and computer tomography (IEC, 62B/416/CD, 2000)". As a result, DQE measurement technique for this thesis was modeled after Gransfors and Aufrichtig (2000), based on work specific to digital mammography, and Dobbins et al. (1995), based on computed radiography acquisition devices.

3.6.1 Methods and Materials

In addition to Equation 3.14, DQE can be mathematically described as the MTF squared divided by the noise of a system, quantified in the noise power spectrum (Shaw, 1963).

$$DQE = \frac{MTF^2}{NPS} \qquad (3.15)$$

Taking into account system-specific parameters, DQE is calculated as a function of spatial frequency (f) and exposure (X) (Granfors and Aufrichtig, 2000):

$$DQE(f,X) = \frac{[S \cdot MTF(f)]^2}{NPS(f,X) \cdot X \cdot C} \qquad (3.16)$$

S is the average signal level, NPS, the noise power spectrum, and C, the x-ray fluence per exposure.

The MTF (Chapter 3), signal level (the average of all pixel values in the region of interest), and exposure were generated for LODOX – MP. Exposure was taken at the surface of the table using an ionization chamber (Model W 23342; PTW) and corrected for detector distance using the inverse square law.

X-ray fluence per exposure (in photons/mm^2/Roentgen), C, varies over the spectrum of x-ray energies. Knowing the energy absorbed per area, a maximized hypothetical C can be derived using the following relationship:

$$C = \frac{E_{abs}}{A} \cdot hv \qquad (3.17)$$

Here *hv* represents the energy of the photons exiting the x-ray tube. The energy used in computing the other parameters of DQE was calculated at 50 kV. Therefore, the maximum energy of x-rays exiting the tube is 50 keV, which generates a fluence value of 284.2 photons/mm^2/μR (Johns and Cummings, 1983). Although LODOX exhibits a particularly hard x-ray beam, this fluence measurement is large considering a C of 280 photons/mm^2/μR equates to an x-ray system with a 7mm of Al HVL (Gransfors and Aufrichtig, 2000). Ultimately, DQE is calculated as a percentage hence the direct relationship between fluence and DQE does not alter the normalized values in the results.

Essentially, NPS measurements are generated by taking the Fourier transform of the region of interest (ROI) of a flat-fielded image (at a given exposure). In accordance with Dobbins *et al.* (1995), information contained in two dimensions is significant; hence a two-dimensional Fourier was used. NPS was computed as the modulus of the two-dimensional Fourier data squared and the magnitude was adjusted to units of mm^2 by multiplying by the pixel pitch over the linear dimension of the ROI (Granfors and Aufrichtig, 2000).

A number of images must be taken at a particular exposure in order to reduce noise. In this case 16 images were averaged to generate the NPS.

3.6.2 Results

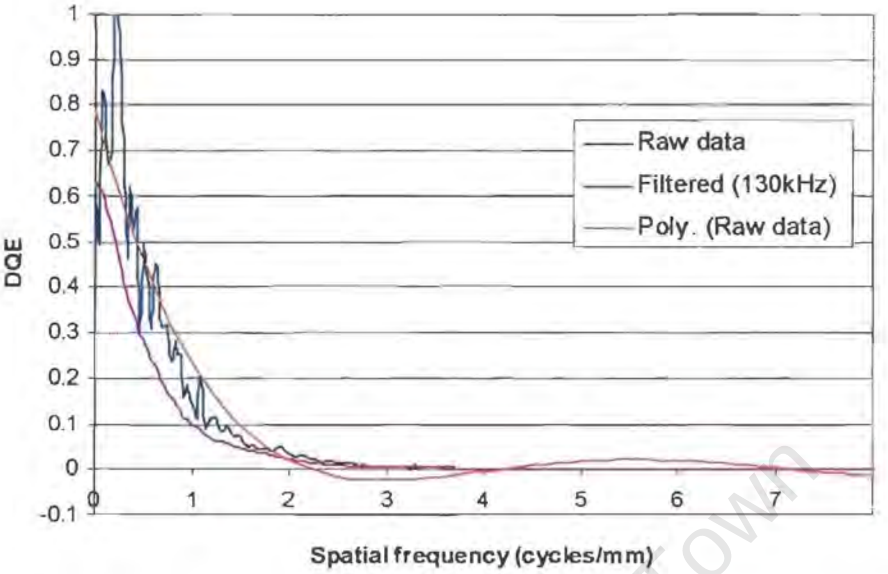

Figure 3.10: LODOX-MP DQE data was analyzed using a 130kHz low pass filter and using a fifth order polynomial best fit treadline.

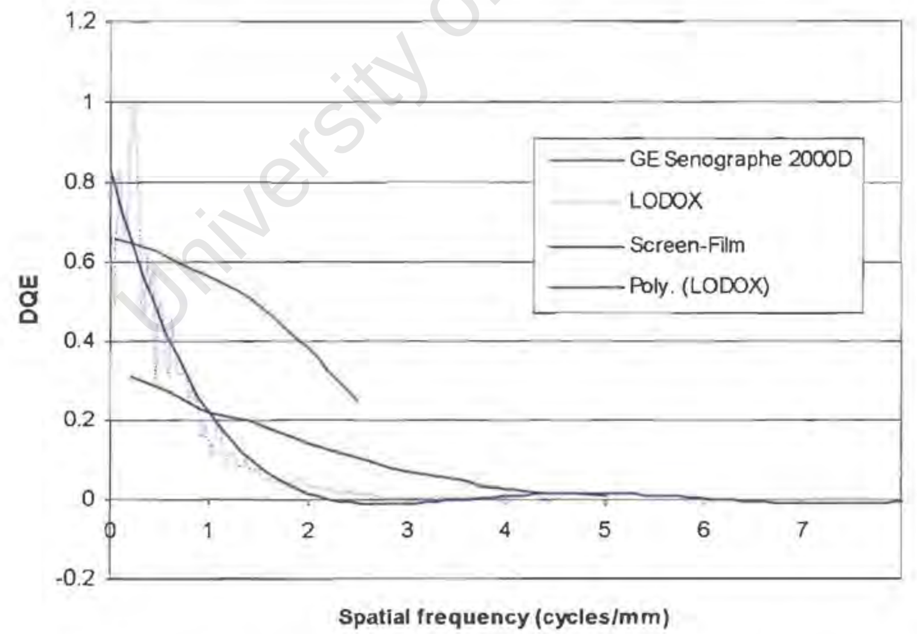

Figure 3.11: Comparison of LODOX DQE and DQE data shown in the literature (Summary of Safety and Effectiveness for GE Senographe 2000D, 2000, and Dobbins *et al.*, 1995).

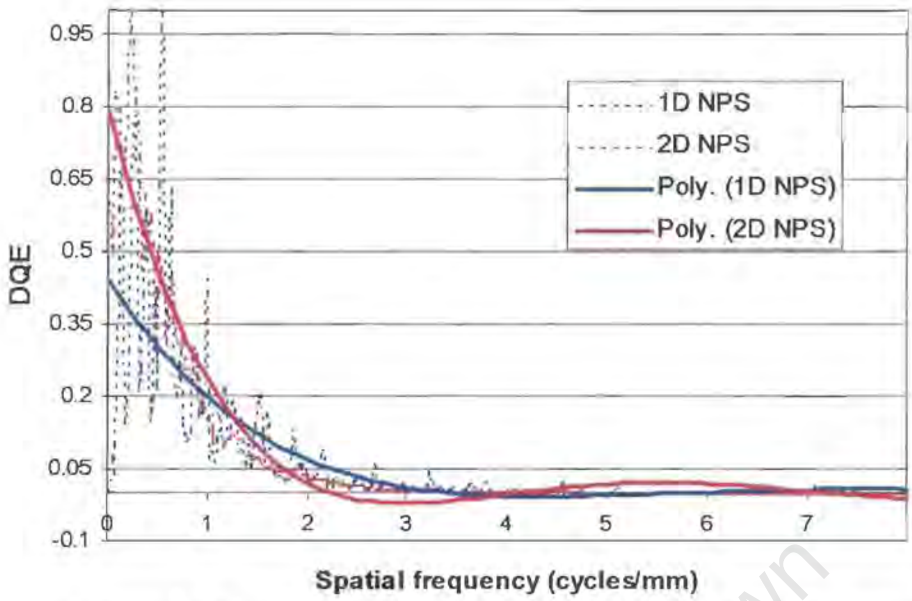

Figure 3.12: Comparison of LODOX DQE calculated with both one- and two-dimensional noise power spectrums (NPS). A two-dimensional NPS is a more accurate representation of noise (Dobbins *et al.*, 1995; Granfors and Aufrichtig, 2000).

3.6.3 Discussion

DQE values are shown above as percent values, in accordance with the literature. In order to eliminate excessive noise, a low pass filter (130 kHz) and a fifth order polynomial equation were fit to the raw DQE. Although the 130 kHz filter was effective in smoothing out the DQE curve, it did not accurately reconstruct the magnitude of the quantum efficiency. The polynomial fit, although not infallible, allowed comparison of LODOX DQE that was more representative of the actual data.

Calculated LODOX DQE was compared to that of a digital mammography system and a digitized screen-film system. Digital mammography data was obtained from the FDA-approved Summary of Safety and Effectiveness Data for the GE Senographe 2000D. Screen-film DQE data is from Dobbins *et al.* (specifically Figure 14b,1995) using a standard system (Philips model SRO 33/100) and computed radiography acquisition device (Philips Medical Systems, PCR model 7000). This particular data was chosen from a number of sets because it illustrated the largest DQE for a pixel size most closely comparable to LODOX.

According to Figure 3.11, LODOX DQE values are higher than the screen-film system at very low frequencies. This indicates that LODOX can detect more incoming photons at a lower radiation dose at a decreased spatial frequency. For frequencies higher than approximately 1.0 cycles per millimeter (using the unfiltered DQE), LODOX quantum noise detection drops below the digitized screen-film system performance. In comparison to the Senographe 2000D, LODOX DQE drops more rapidly over spatial frequencies after approximately 0.5 cycles per millimeter. At 0.5, 1.0, and 1.5 cycles per millimetre, the GE Senographe exhibits DQE values of 0.60, 0.54, and 0.47 (respectively), while the LODOX system at the same spatial frequency only measures DQE values of 0.29, 0.10, and 0.05 (also respectively).

As noted by other authors, a number of difficulties resulted from calculating NPS in this study. Although a 2D representation a NPS provides the best noise description, to compare it to spatial frequency requires a one-dimensional parameter. Dobbins *et al.* (1995) also processed a one-dimensional slice of the NPS to generate a one-dimensional representation. To determine the effects of this, LODOX DQE was also calculated using a 1D NPS (Figure 3.12). Although the DQE based on a one-dimensional NPS illustrates better quantum efficiency at higher spatial frequencies, it does not accurately include both dimensions of noise.

A number of factors that degrade DQE (Gransfors and Aufrichtig, 2000) include incomplete x-ray absorption, secondary quantum noise, spatial variation of gain, additive system noise, and aliasing (quantified in the MTF). Absorption of different x-ray photons results in different amounts of signal (Swank factor (Swank, 1973)) and different point spread functions (Lubberts effect (Lubberts, 1968)), which also obscure the DQE.

LODOX DQE values are also at a disadvantage when compared to the GE Sensographe because LODOX is not a mammography specific system. LODOX has a larger inherent filtration (due to tube filtration plus a glass window) thus a greater proportion of low energy x-rays are removed from the beam (see Chapter 3). The resulting high energy x-rays contribute to quantum noise because they are absorbed with less quantum efficiency than the lower energy x-rays normally utilized for mammography. Likewise, the scintillator currently used for the LODOX-MP is optimal for x-ray absorption in the 100 kV range however it allows more photon spreading than mammography-specific scintillators (primarily due to thickness). Scintillator thickness is discussed in Chapter 5.

3.7 Mammography Phantom Comparisons

Mammography phantoms were used to compare the mammographic image quality of the LODOX-MP with a standard screen-film mammography system. The GE Senographe 600T at the Groote Schur Radiology Department was utilized for this analysis. The machine was manufactured in January 1990, exhibits 0.8mm of Be filtration, and a 0.1-0.3 mm focal spot. Standard clinical mammograms on this machine are taken at energies between 24-33kV.

3.7.1 Materials and Method

The RMI Mammographic Accreditation Phantom Model 156 was used to compare image quality of screen film mammography with digital LODOX images. This phantom fulfills the standard of image quality required by the American College of Radiology (ACR) and uses the criteria of specified fibrils, filaments, and simulated microcalcifications. The base is composed of acrylic (3.3cm thick) and test objects, imbedded in wax, are enclosed inside with an additional 0.3 acrylic cover. The phantom attenuates x-rays with the same characteristics as a 4.0-4.5cm breast composed of 50% adipose tissue and 50% glandular tissue.

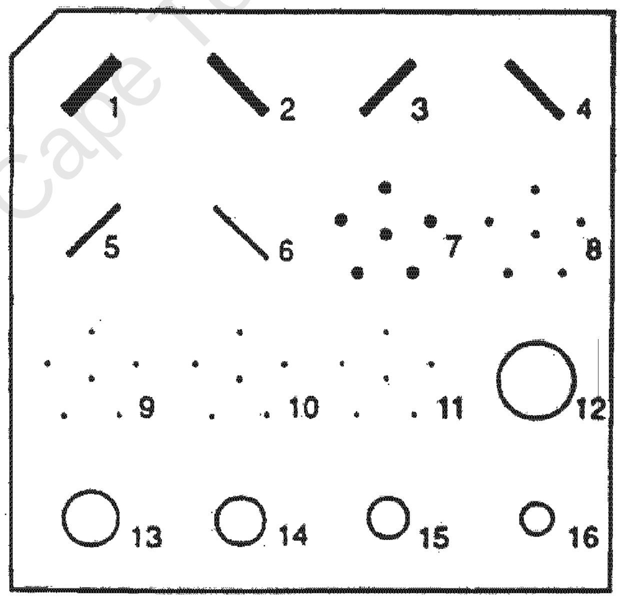

Figure 3.13: Layout of lesions, rods, and microcalcifications in Accreditation Phantom Model 156.

The Dupont processed phantom system contains multiple components (see Appendix I). Acrylic absorption components are assembled around a black imaging grid that contains microcalcifications, wires, spheres, minimal detail-contrast disks, and tumor simulations.

Both phantoms were imaged at the optimal energy based on thickness as selected by the radiographer (27 kV). The screen-film system mechanically selects its own x-ray intensity using Automatic Exposure Control (AEC). The Model 156 Phantom was imaged twice (with either Al or Mo filters) at the system's highest energy (35 kV) to generate the most representative peak energy of the LODOX-PPM. Similar images of the phantoms were taken at 40 kV to stimulate the most accurate mammographic x-ray energy, and a large range of intensities (64 – 320 mAs) was used for inclusiveness.

	Test Object	Score
1	1.56 mm nylon fibre	1
2	1.12 mm nylon fibre	1
3	0.86 mm nylon fibre	3
4	0.75 mm nylon fibre	5
5	0.54 mm nylon fibre	9
6	0.40 mm nylon fibre	10
7	0.54 mm microcalcification	1
8	0.40 mm microcalcification	1
9	0.32 mm microcalcification	6
10	0.24 mm microcalcification	7
11	0.16 mm microcalcification	10
12	2.00 mm tumour-like mass	1
13	1.00 mm tumour-like mass	1
14	0.75 mm tumour-like mass	1
15	0.50 mm tumour-like mass	7
16	0.25 mm tumour-like mass	10

Table 3.8: Recommended scoring system for the Accreditation Phantom Model 156.

Screen-film images were read with an experienced radiographer in an x-ray room using luminescence view box display and a magnifying glass in a darkroom (customary procedure for screen-film mammograms). LODOX phantom images were read as a soft-copy from the display monitor and contrast and brightness was adjusted to optimize object detection.

Objects in the ACR Accreditation Phantom Model 156 were scored according to designated criteria (provided with the phantom), where objects are weighted based on detection difficulty.

3.7.2 Results

Image	kV	mA	lesions	rods	specks
LODOX	40	64	1	0	0
LODOX	40	80	1	0	2
LODOX	40	100	1	0	2
LODOX	40	125	1	0	2
LODOX	40	160	3	1	2
LODOX	40	200	3	1	2
LODOX	40	250	3	1	2
LODOX	40	320	3	2	2
SF	27	AEC	20	10	2
SF	35	AEC	4	3	2

Table 3.9: Comparison of Screen Film (SF) and LODOX images of ACR Accreditation Phantom Model 156. Images are scored according to literature criteria.

Image	kV	mA	row A	row B	row C	row D
LODOX	40	64	1	3	2	3
LODOX	40	80	2	3	2	3
LODOX	40	100	2	4	3	4
LODOX	40	125	2	4	3	4
LODOX	40	160	2	4	3	4
LODOX	40	200	2	4	3	4
LODOX	40	250	2	4	3	4
LODOX	40	320	3	4	4	5
SF	AEC	27	3	4	4	5

Table 3.10: Comparison of screen-film and LODOX images of DuPont mammographic test phantom. Numbers represent the maximum row of visible objects.

3.7.3 Discussion

Of the screen-film images, the image that exhibited the best clarity was taken at 27 kV with a Mo filter. The Model 156 film taken at 35 kV appeared slightly overexposed, and clarity was sacrificed to the brightness of the image. The Dupont phantom demonstrates the most lucidity and variability in objects and as a result, was useful for comparison with digital images.

In screen film mammography, exposure is automatically selected via calibrated sensors under the film cassette. This prevents over-and under-exposure of films because there is no direct correlation between breast thickness, compressibility, radiographic density and size (Kopans, 1998). According to Huda and Sloan (1995), typical mammography x-ray tubes range from 80-100mAs, and exposure times are usually about 1 second. For this study, exposure readings were taken over one second at intensities between 80-125mA. As a result, the images generated at 80 and 100 mAs should be representative of screen-film intensity.

Comparisons of LODOX and screen-film films for both phantoms illustrate LODOX's deficiency as a mammographic imaging system. This is expected because LODOX was built for general radiography purposes. A problem with these comparisons is the divergence in x-ray energy of the two systems. Because LODOX is imaging at 40 kV (its lowest possible energy), the high energy x-rays are being transmitted through the phantom with little absorption. According to the measured HVL, LODOX beams are also particularly hard. As a result, image resolution is less than the screen-film system. To utilize LODOX technology for mammography, x-ray tube selection must be specifically in the mammographic range. X-ray energy and other LODOX tube parameter alterations discussed in Chapter 5.

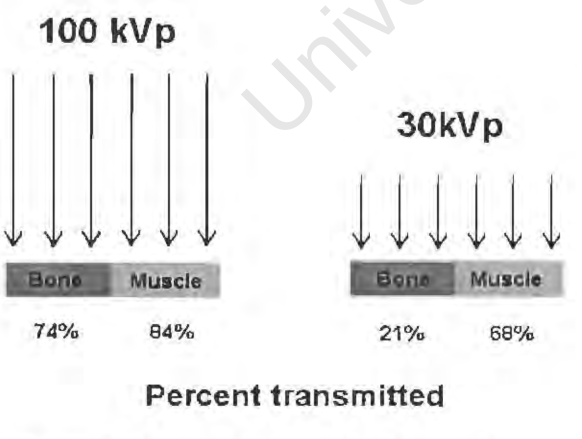

Figure 3.14: Illustration of attenuation differences between muscle and bone at various x-ray energies. Breast tissue (0.98g/cc) and muscle (1.0g/cc) have similar densities. Picture adapted from Huda and Sloan (1995).

The LODOX scintillator is also much thicker than a dedicated mammography scintillator because it was selected for a 100+ kV range. High energy x-rays require a thicker scintillator to stop and absorb them however, this is not necessary for mammography. As a result, the excessive scintillator thickness degrades spatial resolution because it allows more spreading of the light. In comparison to imaging bone and muscle in general radiology, imaging breast tissue requires greater resolution due to smaller differences in attenuation.

Chapter 4

LODOX Radiation

4.1 Introduction

The possibility of radiation-induced tumour malignancy has been repeatedly explored, specifically in dealing with the sensitive glandular tissue of the breast (Boise, 1979; Webster, 1979). It has been estimated that 1rad of absorbed radiation to the tissue of the breast would increase the risk of cancer by 1% (Andolina *et al.*, 1992). Some studies, such as those of female atomic bomb survivors in Hiroshima and Nagasaki, have shown that radiation at exceedingly high exposure can induce breast cancer (Tokunaga *et al.*, 1987, Preston *et al.*, 1987).

The acceptable amount of radiation delivered during a standard mammography screening, in comparison, is less than 100 to 4,000 times the radiation absorbed in an atomic explosion. At the accepted radiation dose (less than 0.3rads or 3mGy), there is very little risk for screening women over the age of 40 (Mettler *et al.*, 1996). However, it is still necessary to quantify the amount of risk involved in screening the sensitive tissue of the breast.

Accurately measuring radiation dose in mammography can be difficult because related photon interactions at a low energy range (below 50keV) are quite complex (Doi and Chan, 1980). To determine the energy imparted to breast tissue during a LODOX scan, different classifications of radiation must be defined. The conventional term *dose* can be described by terms such as *entrance dose*, *absorbed dose*, *mean breast dose, mean glandular dose*, and *effective equivalent dose*.

Exposure is the term that identifies the quantity of x-rays that cause a certain charge to be produced in a block of air of a designated mass. Essentially, exposure is a measure of the ability of radiation to ionize air. According to the 1962 report of the International Commission on Radiation Units and Measurements, exposure is measured in Roentgen (R) as follows:

“the exposure (X) is a quotient ΔQ by dm, where ΔQ is the sum of the electrical charges on all the ions of one sign produced in air when all of the electrons, liberated by photons in a volume element of air whose mass is Δm, are completely stopped in air:

$$X = \Delta Q/\Delta m$$

The special unit of exposure is Roentgen (R). 1 R = 2.58×10^{-4} C/kg (exactly).”

This quantity is usually used to describe the energy output of the x-ray generator and can be measured by a thermoluminescent dosimeter (TLD), consisting of chips of lithium floride, or an ionization chamber using dose-to-exposure conversions.

Patient *entrance dose* is often used to describe the amount of radiation that impacts the patient’s skin. Entrance dose describes the intensity of the x-ray beams, thus the amount of current flowing through the x-ray tube affects this parameter. Conversion of exposure to entrance dose can also be computed using normalized dose factors (Johns and Cunningham, 1983) such as those used by Hammerstein *et al.* (1979) and Doi and Chan (1980) for mammography.

Absorbed dose measures the transfer of energy from high energy electrons to a medium through excitation and ionization. Absorbed radiation dose is a function of beam quality, depth, and surface exposure (Hammerstein *et al.*, 1979). Nearly half a century ago the ICRU explicitly defined the unit of absorbed dose as the rad in its 1956 and 1962 reports.

“The absorbed dose (D) is the quotient of ΔE by Δm, where ΔE_D is the energy imparted by ionizing radiation to the matter in a volume element, Δm is the mass of matter in that volume element.

$$D = \Delta E_D/\Delta m$$

The special unit of absorbed dose is the rad. 1 rad = 100 erg/g = .01J/kg”

This unit was specifically created to measure the amount of radiation absorbed by soft tissue (Fullerton *et al.*, 1980). The SI equivalent to the rad is the gray (Gy), where one gray is equal to one joule per kilogram. Absorbed dose can be calculated as a function of depth or through a quantification of total energy imparted. Thus, the term *mean breast dose* is used to describe the average dose for a particular breast thickness.

In mammography, the amount of radiation absorbed by the glandular tissue is the most pertinent due to its sensitivity to radiation. For this study, the *mean glandular dose* per unit exposure (in air) to the average breast will be calculated by dividing the total energy absorbed in the breast by the total glandular mass. Although significant amounts of energy are absorbed in the skin, fat, and connective tissue of the breast, they are not at high risk at low levels of radiation (Hammerstein *et al.*, 1979). This is also a key measurement required by the American College of Radiology (ACR) Mammography Accreditation Program.

The term *effective equivalent dose* takes into account the efficacy of the x-rays in causing physiological damage. This measurement is based upon the amount of radiation that is permissible to the entire body. An organ weighing factor is used to account for partial body irradiation that manifests the organ's sensitivity to the received dose.

4.2 Quantifying Exposure

Although exposure at the skin is not an accurate measurement of total patient dose (Doi and Chan, 1980; Hammerstein *et al.*, 1979), this measurement was used in this study for the determination of beam quality (Chapter 3) and various radiation doses. Although relative readings may be used to quantify beam quality, exposure readings were chosen to attain both half value layer measurements, and absorbed dose calculations. Entrance exposure in particular is useful for generating dose comparisons at a particular tissue depth.

Exposure relates the number of ion pairs (of a single sign) that are liberated by photons in an air mass (Johns and Cunningham, 1983). Using the x-ray spectrum generated at a voltage V with discrete energy bins $\Phi(E)$, the exposure in air of an x-ray spectrum can be calculated using the following equation from Gkanatsios and Huda (1997):

$$X = \frac{e}{W}\sum_{E=1}^{V}\frac{\mu_{ab}(E)}{\rho_{air}} E\,\Phi(E) \quad \text{C/kg} \qquad (4.1)$$

W represents the ionization energy of air (33.97 eV per ion pair), e is the unit charge (1.602e-19 C), Φ equates to the photon fluence (in photons per cm^2), and $\mu_{ab}/\ \rho_{air}$ signifies the absorption energy coefficient of air (in m^2/kg), also known as the mass energy absorption coefficient. Exposure X given in C/kg can be equated to Roentgen with the following conversion: 1.0R = 2.58E-4 C/kg. Assuming a monoenergetic photon source, exposure can also be given by (Gkanatsios and Huda, 1997):

$$X(hv) = (3.876E10)\left|\frac{\mu_{ab}}{\rho_{air}}\right|_{hv} \frac{e}{W} hv\Phi(hv) \quad \text{Roentgen} \qquad (4.2)$$

Equations from Tucker (1991) can be used to generate $\Phi(hv)$ for x-ray tube voltage ripple factors ranging from 0 to 100%, constant potential to single phase respectively. The Voltage Ripple value published for LODOX technology is 0.5% (Booysen, 1998), with a Ripple Stability value of less than 4%. X-ray generators with ripple factors ranging from 0% to 20% will result in minimal errors (between 0% and 2%) when calculating the energy imparted at any given HVL and kV (Gkanatsios and Huda, 1997).

Mass attenuation coefficients describe the fraction of penetrating photons that are "lost" by an x-ray beam when traveling through a mass of material. A parameterized model for determining the mass attenuation coefficients has been published by Tucker *et al.* (1991) to accurately describe the coefficients of various elements and energies:

$$\frac{\mu}{\rho}(u) = \alpha_1 + \alpha_2 u^{-1.6} + \alpha_3 u^{-2.7} + \alpha_4 u^{-3.5} + \alpha_5 u^{-4.5} \qquad (4.3)$$

The value of u is equal to $hv/100$, where hv is the photon energy in keV. The parameters α_1–α_5 are measured at m^2/kg. The attenuation coefficients that are used for x-rays between 5 to 50keV can be viewed in Table 4.1. Aluminium, tungsten, and rhodium are common target materials and air is listed because its attenuation coefficient is used in calculating exposure (Equation 4.3).

Material	α_1	α_2	α_3	α_4	α_5
Al	1.734E-2	-1.918E-3	3.133E-3	4.457E-4	-9.447E-6
$W(hv<E_k)$	-8.879E-2	1.231E-1	1.229E-2	2.209E-2	-1.673E-3
$W(hv>E_k)$	-2.849E-2	3.600E-1	-4.539E-3	7.621E-1	-1.977E-
$Rh(hv<E_k)$	-8.746E-2	1.331E-1	3.210E-3	2.892E-2	-2.259E-3
$Rh(hv>E_k)$	-1.191E-2	1.832E-1	6.708E-2	3.004E-1	-8.137E-2
Air	1.447E-2	1.182E-3	1.547E-7	1.367E-4	-2.227E-6

Table 4.1 Parameterization Coefficients for Target Materials taken from Gkanatsios (1995)

In Table 4.1, the E_k values are equated with the K edges of tungsten and rhodium (69.5 and 71.5 keV, respectively). The most constructive value generated from this data for this study is the attenuation coefficient for tungsten below the E_k value. From Chapter 3, the average energy of photons exiting the LODOX-MP tube at 40 kV was determined to be 27.14 keV. Using the coefficients above and assuming a photon energy value of 30keV, the attenuation coefficient for the LODOX tungsten target is calculated to be 2.26 m^2/kg. However, this calculation applies to monoenergetic x-rays, and thus energy must be summated for each contributing photon equivalent energy (keV) or the average keV must be used.

LODOX has a relatively high HVL (4.04 mm of Al at 100 kV, versus 3-3.5 mm Al for typical diagnostic machines) illustrating that x-rays of a given kV value have a greater potential to reach their peak energy in keV. As a result of strong penetrability, the average energy of the LODOX x-rays exiting the tube is higher than standard radiography machines. As a result, either an exposure meter (or in this case dose meter) is employed for the purpose of summing the contributing x-ray energies to determine the ability of ionization.

Exposure measurements were taken in this study using a UNIDOS PTW dosemeter. The amount of electric charge collected in a 0.02cc ionization chamber (in C) was equated to Roentgen using standard conversion factors from Johns and Cunningham (1983). Since exposure is a necessary parameter of HVL, entrance dose, and absorbed dose, exposure readings are listed in these sections of Chapters 3 and 4.

4.3 Average Glandular Dose

Energy absorption in biological tissue is a two-stage process. Firstly, electrons are set into motion by the photons that bombard them, and second, the electrons escape from their atoms and release energy while they travel through a substance. These electrons lose their energy by ionizing atoms along their paths (Johns and Cunningham, 1983). The first stage results in the measurement of kerma (Kinetic Energy Released in the Medium) of the interaction, while the second results in the absorbed dose.

The amount of radiation dose present at the surface of an imaged object has indirect relevance to the biological harm of an imaging system. Although entrance dose does not quantify the energy imparted to the body, an accurate assessment of surface dose is necessary for forming a correlation between depth and absorbed doses (Hammerstein *et al.*, 1979).

Absorbed dose, a measure of the total energy absorbed in the breast tissue, is a relative indicator of risk in mammography. As opposed to entrance dose, quantifying the resultant radiation from a single breast scan provides an absolute factor for radiation dosimetry comparison. Calculation of the absorbed dose to glandular tissue is a more direct measure of risk, because cancers initiate from the glandular and ductal epithelium of the breast (Kopans, 1998; Hammerstein *et al.*, 1979).

Calculation of the average glandular dose (AGD) is necessary to compare dose imparted to acceptable ACR standards. AGD can be calculated by dividing the average dose per unit exposure by the mass of glandular tissue that is receiving radiation. Measures of skin entrance dose (or surface exposure) and beam quality are fundamental in calculating AGD (Kopans, 1998). Because dose varies with depth, it is not possible to measure the mean glandular dose directly however, by using a phantom it is possible to estimate average glandular dose *in vivo* knowing the HVL.

4.3.1 Methods and Materials

To calculate the mean glandular dose, the average normalized glandular dose (D_{ng}) was generated from data of Stanton *et al.* (1984), as a function of LODOX HVL at 40 kV (1.59 mm of Al) and breast thickness (see Appendix D). These values are used to calculate average glandular dose (AGD) as a function of breast thickness. In this case X represents surface exposure.

$$AGD(z) = D_{ng}(z) * X \tag{4.4}$$

Again, HVL was used to describe the quality of the LODOX beam because the inherent energy of the x-rays is not dependent upon the peak kV setting of the x-ray tube.

4.5.2 Results

Intensity	**Exposure**	**4cm**	**5cm**	**6cm**	**7cm**
mA	*Roentgen*	*rad*	*rad*	*rad*	*rad*
70	0.036	0.022	0.020	0.019	0.017
80	0.045	0.028	0.026	0.023	0.021
100	0.057	0.036	0.033	0.030	0.027
125	0.069	0.043	0.040	0.036	0.033
160	0.084	0.053	0.048	0.044	0.039

Table 4.2: Average glandular dose calculated on the basis of HVL and entrance exposure over a range of mammographic intensities.

4.3.3 Discussion

The average glandular dose calculated for a single scan increases as the intensity of the x-ray beam increases (as would be expected). The average glandular dose decreases as a function of breast thickness because a larger amount of tissue is absorbing the energy imparted to the breast. As stated previously, the acceptable value per image by the ACR is 0.3 rads. LODOX, at its current configuration, exhibits average glandular doses that are approximately 10 x an order of magnitude smaller than the acceptable ACR value (between 13.4-5.7 times lower) throughout the range of x-ray intensities for a 4cm breast. The ACR mean glandular dose is based on a phantom 4.5cm thick, composed of 50% fat and 50% glandular tissue.

With respect to ACR glandular dose requirements, the data above suggests that the low doses delivered to breast tissue by LODOX are more than acceptable for mammographic procedures. However, the image quality provided by LODOX technology is not acceptable for mammography. Thus, adjustments to improve image quality while maintaining the present low average glandular dose would provide the best possibilities for a LODOX mammographic system.

Chapter 5

LODOX Mammography Considerations

5.1 Introduction

The LODOX - MP is currently not capable of producing mammographic scans with image quality comparable to screen-film systems. However, these mammographic shortcomings have been analyzed to determine what alterations can be utilized to create LODOX technology suitable for breast cancer detection. The LODOX - MP does however deliver a radiation dose that is approximately ten times lower than acceptable glandular mammography doses. Thus, the utilization of LODOX technology for breast imaging is still feasible with image quality improvements, provided these augmentations do not raise the patient risk.

5.2 Summary of Findings

It is evident from the phantom studies (particularly the ACR Accredation Model 156) that LODOX cannot detect microcalcifications, rods, and lesions with the same accuracy as a screen-film system. In many cases the objects in LODOX phantom images were not observable with contrast and brightness adjustment. As stated in the discussion, the LODOX system is not optimized for imaging in the mammographic energy range. As a result, the scintillator is thicker than those used in mammography because it was selected to absorb higher energy x-rays. The attenuation properties of a mammography phantom are also not designed for image analysis with high energy x-rays. A majority of hard x-rays are transmitted through the phantom without absorbing, and creating useful information at the detector. Attenuation characteristics of the breast are unadjustable however, the LODOX scintillator thickness can indeed be altered. Scintillator suggestions are discussed in the Equipment section of this chapter.

Quantification of LODOX beam quality at 40kV illustrated the hardness of the emitted x-ray beam. The high HVL measured for LODOX (1.59 mm of Al at 40kV) far exceeds the optimal HVL of mammographic systems (0.3 – 0.4 mm of Al). Fortunately, beam hardness is an adjustable parameter that can be manipulated by filtration. The LODOX tube maintains a larger inherent filtration than mammography systems which removes the soft energy x-rays useful for breast imaging. To optimize LODOX technology for breast imaging, tube considerations, such as filtration, are also discussed in this chapter. Preliminary beam measurements performed in the half value layer analysis also illustrated the absence of the Heel Effect in the LODOX imaging. Due to LODOX scanning configuration, uniform intensity of the x-ray beam, which does not occur in standard mammograms, is unique to scanning systems such as LODOX.

Quantification of image parameters such as modulation transfer (through MTF) and quantum efficiency (through DQE), suggest improvements could be made to increase object detectability in order to make LODOX technology sufficient for breast exams. In accordance with criteria of Williams *et al.* (1997), LODOX is nearly capable of a 5% modulation transfer function at 8-10 cycles/mm, as is recommended for digital mammography systems. Similarly, a graphical comparison of LODOX MTF at low energy illustrates that the LODOX-MP transmits modulation with just slightly less efficiency than the best digital mammography system on the market (GE Senographe 2000D). However, from the MTF it was possible to estimate the limiting spatial resolution (LSR) of the LODOX – MP. This value (~4.5 lp/mm) is not sufficient to FDA standards for screen-film mammography (11 lp/mm). Likewise, a graphical comparison of DQE illustrates that LODOX-MP detects quantum noise better than screen-film systems only at very low spatial frequencies (less than 1 cycle/mm).

Imaging parameters of LODOX that illustrate the benefits of a digital scanning imaging system, such as contrast, and favorable scatter ratios, again emphasize the feasibility of LODOX breast imaging. For example, the inherently larger contrast range of digital systems, as opposed to the narrow exposure latitude of screen-film systems, is superior due to adjustability on the soft-copy display. The low scatter to primary ratio (SPR), resulting primarily from using a scanning beam (smaller field of view), illustrates that LODOX maintains less scattered x-rays than standard mammography systems (cone beam systems). A low SPR (0.2 for LODOX versus 0.29-0.59 for standard mammography) also advocates that compression may not be necessary because its foremost function is to reduce scatter. Although the elimination of compression would increase the patient dose, the reduced dose delivered in a LODOX scan is already exceptionally low. However, the elimination of compression would cause increases in focal spot blur, breast motion, and tissue overlap. These issues would have to be addressed and tested in order to determine if the elimination or at least lessening of compression would be feasible for a LODOX-type mammogram. Mechanical design options without compression are discussed in a later section of this chapter.

LODOX radiation doses, are comparable to the mammographic dose range. The LODOX dose that would be delivered to the sensitive glandular region of the breast fulfills the criterion set by the American College of Radiology. At 80 mA-s, an exposure range common to screen-film mammography, the mean glandular dose is ten times less than the value required by the ACR (0.028 rad compared to 0.300 rad). This criterion was still markedly fulfilled at higher x-ray intensities.

5.3 Tube Recommendations

5.3.1 X-ray range

The spectrum of x-rays used in the mammogram (i.e. the *radiation quality*) affects the subject contrast. Tube target material, kilovolt setting, and filtration determine the distribution of x-ray energies. Photoelectric absorption is the primary source of x-ray absorption in soft tissue below 50 keV (Johns and Cunningham, 1983), the necessary range for breast imaging. X-rays that are too high in energy are often transmitted through the breast without generating useful information at the detector or film, while x-rays that are too soft contribute to higher dose when absorbed by the breast.

To be useful for breast imaging, the LODOX system x-ray tube should be specific for the different x-ray requirements necessary for mammograms. As stated previously, breast tissue has inherently low contrast and thus requires x-rays of with nominal energy. In the LODOX-MP, the x-ray generator has an x-ray energy range from 40-135 kV, which can be adjusted at 10kV increments. A dedicated mammography unit would have to utilize a lower range of x-rays (24-36 kV) and be operative at one kilovolt increments.

5.3.1 Tube target/filter composition

The target material used in the x-ray tube is an important consideration for any type of x-ray system because photon production in the x-ray tube is derived from interactions of the electrons with the anode (producing *characteristic radiation* and *bremsstrahlung radiation*). Molybdenum, rhodium, and tungsten are common metals used for both the target and the filter of current screen-film mammography systems. A molybdenum target and filter of 0.03mm (standard for mammography) creates a narrow energy spectrum between 17 keV and 20 keV. In contrast, rhodium and tungsten anodes generate a larger proportion of higher energy photons

For a digital mammography system, it is beneficial to use x-ray beams that are higher in voltage than those used in screen-film. This is due to the larger contrast range and adjustability of digital systems, and particularly soft-copy display. Although molybdenum is the most common anode target and filter for current mammography systems, Kopans (1998) recommends tungsten for a primary digital system because digital imaging does not experience the contrast differentiation problems that screen-film systems exhibit. Haus and Yaffe (2000) also prefer tungsten and rhodium (with Al filtration) over molybdenum for targets and filters in the x-ray tube. Thus, the preferred x-ray tube for LODOX-type mammography would employ a rhodium or tungsten target.

The x-ray spectrum of a tube can be refined using filters to narrow the range of photon energies that are allowed to pass through. A small energy range of x-rays is advantageous because it creates better contrast from photons at lower energies. To be useful for breast imaging, the inherent filtration of the x-ray tube should create an optimal window of x-ray energies (between 24-32 kV).

Additional beam filtration occurs as the x-rays exit the tube through a window. L-shell x-rays have characteristically low energy and for normal radiographic systems, are usually absorbed by the window of an x-ray tube (Huda and Slone, 1995). A beryllium window, specific to mammographic systems, allows a majority of these x-rays to pass through. Along with the actual tube voltage range, an imperative modification for a LODOX mammographic prototype is the window of the x-ray tube. A standard radiographic imaging x-ray tube, such as the one used in LODOX, possesses a glass window which absorbs a major portion of the low energy x-rays which are useful in breast imaging. The implementation of a beryllium window reduces the amount of unnecessary filtration by the window and the image clarity is not hindered.

5.3.2 Anode rotation, angle, and focal spot

LODOX technology utilizes a rotating anode in order to dissipate the heat generated by the electrons hitting the anode target. As a result, the current can be higher, which reduces the exposure time (Andolina et *al.*, 1992). The disadvantage to rotating anodes is the increase in off-focus radiation however, incorporating a diaphragm in the tube housing can eliminate the unwanted off-focus radiation. Due to the sensitivity of breast tissue to radiation, a rotating anode is recommended for mammography specific LODOX technology.

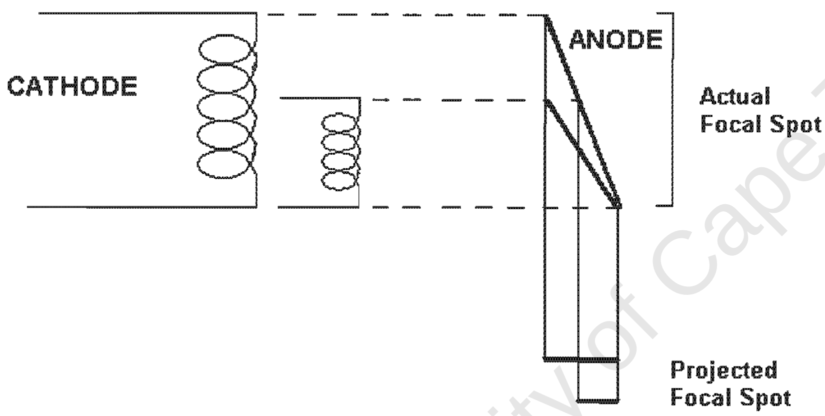

Figure 5.1: The *actual* or *target focal spot* is the area on the anode where the accelerated electrons actual strike the target surface. The *projected focal spot* is smaller than the anode spot due to the angulation of the x-ray source. Incident electrons concentrated in a small area would melt the anode at that particular location.

Anode targets are angled to decrease the projected focal spot without compromising tube durability (a larger electron impact area allows for better heat dissipation). The optimal anode angle of a mammography tube is between 6-18 degrees. The positioning of the x-ray tube axis in a dedicated mammography system is based on the fact that a large Heel Effect exists. Heel Effect is addressed in Chapter 3. It is evident that the large SID and small field size (using a narrow beam instead of a cone) of LODOX-MP result in no observable Heel Effect. The tube angle determines what portion of the beam that is utilized and equipment requirements insist that the central beam of the x-ray tube is parallel with the chest wall (Diagnostic X-Ray Imaging Task Group No. 7). As a result, a mammography tube axis is tilted and collimated so that only half the beam actually reaches the breast. Since LODOX employs scanning technology (a line beam rather than a scanning beam), tube axis angulation is unnecessary for an x-ray tube in order to optimize breast imaging.

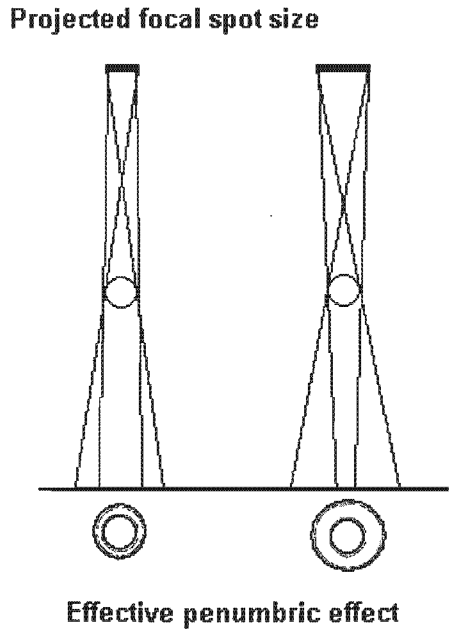

Figure 5.2: A comparison of penumbric magnitude illustrates the benefit of a small focal spot.

A penumbra results from a finite focal spot size. When photons reach the front of an object they cast a shadow on the detector plate as they diverge from the focal spot and cross one another. A small focal spot is an essential characteristic of good image resolution however (Figure 5.2), this feature is held in check by the heat loading capacity of the anode (Kopans, 1998). If the focal spot were too small, heat would concentrate in a particular area of the anode and would be more prone to melt. The angling of the anode allows for a more concentrated focal spot while spreading the heat over a larger area. This way, the anode is less likely to melt, and a smaller focal spot size is generated.

In standard mammographic units, the nominal (actual) focal spot size is 0.3mm for most screening procedures. For magnification images, more typically for diagnostic mammography procedures, a secondary nominal focal spot (0.1mm) is used (Haus and Yaffe, 2000). When using the term nominal focal spot size, it must be noted that this convention allows the actual distribution of radiation to be 1.5 to 2 times larger than the nominal value. The effective or projected size is largest near the chest wall (the location of the central x-ray), but varies over the surface of the image.

5.3.4 Tube comparison

Compared in Table 5.1 are important parameters of LODOX x-ray tubes (Varian G1582BI and Varian A2582BI) and a standard mammography x-ray tube manufactured by the same company (Varian M151). Likewise, an industrial tube that also uses a beryllium window (Brand X-ray tube BX-2) is listed for comparison. The M151 is marketed as a direct replacement mammography tube.

Characteristics	Varian A2582BI	Varian G1582BI	Varian M151	BX-2
Load Ratings	41kW	60kW	4kW	N/A
Focal Spot	0.6mm	0.6mm	0.3mm	0.5mm
Target Material	Tungsten	Tungsten	Molybdenum	Tungsten
Target Angle	10 degrees	10 degrees	12 degrees	12 degrees
Nominal Tube Voltage	125kV	125kV	49kV	40kV
Max.Recommended Filament Current	N/A	5.2A	5.5A	2.2A
Anode Speed	2800rpm	2800rpm	2850rpm	N/A
AccelerationTime for Rotation	11sec	3-5sec	N/A	N/A
Anode Diameter	184mm	133mm	70mm	N/A
Max. Anode Heat Content	1853kJ	1111kJ	65kJ	225kJ
Max. Anode Heat Dissipation	3kW	2.83kW	N/A	125kW
Inherent Filtration	None	None	0.8mm Be	0.25mm,0.5mm
Window	Glass	Glass	beryllium	beryllium

Table 5.1: Comparison of various commercial x-ray tube parameters.

For mammographic images, the optimal tube utilized for LODOX would involve the considerations discussed above. Especially significant parameters include the smallest available focal spot, low energy range with a narrow range, a beryllium window, and filtration sufficient for a 0.3-0.4 mm of Al half value layer. Additionally, the x-ray tube should allow increments of 1kV, which is required by United States Food and Drug Administration and European Commission standards. Mammography-specific x-ray tubes which support these configurations are available on the commercial market however, a tube specific to a scanning beam would not require the same tube axis tilt used in cone beam systems.

5.4 Scintillator Recommendations

An x-ray scintillator converts absorbed x-rays into visible light in the blue to green region of the spectrum. Scintillators can be composed of a variety of materials, each of which maintain different x-ray-to-light conversion qualities. Significant characteristics of a scintillator include (1) the fraction of x-ray energy absorbed, (2) the fraction of absorbed x-ray energy converted to light, (3) the fraction of such light usefully emitted (scintillator efficiency), and (4) the point spread function of the composite layer (Wells, 1982).

Substance and main application	**Colour**	**Typical fraction of x-rays absorbed (η_a)**	**Fraction of absorbed x-rays emitted as light (η_e)**	**Figure of merit ($\eta_a\eta_e$)**
Zn, CdS: Ag Traditional fluoroscopy, image intensifiers	Green	0.25	0.15	0.04
$CaWO_4$ Radiography	Blue	0.45	0.03	0.015
CsI:Na (evaporated) Image intensifiers	Blue	0.6	0.10	0.06
Gd_2O_2S:Tb Radiography	Green	0.6	0.15	0.09

Table 5.2: Typical screen materials and their properties (taken from Wells, 1982). The LODOX-MP scintillator is composed of Gd_2O_2S:Tb, a material also used in some mammographic systems.

The active portion of a fluorescent screen consists of a layer of powdered crystals that often include impurity atoms to introduce free electrons into the crystalline lattice. For example, the LODOX scintillator is composed of Terbium doped Gadolinium Oxysulfide. This powder is mixed in epoxy glue and laid over a plastic sheet for rigidity. The crystals in the screen absorb the x-ray energy in the form of quanta. As a result of quantum absorption the energy levels of the free electrons is raised. Visible light is then emitted when the electrons return to their original energy levels. Light emitted in the forward direction is collected by film (as the detector) or a charge coupled device (CCD), in the case of LODOX, to create an image. Light directed backwards can be partially reflected by the substrate, and some emerges in the forward direction. The color of the light is characteristic of the crystal lattice composition.

5.4.1 Scintillator Efficiency

A scintillator's ability to convert x-rays to visible light depends on the composition, thickness, and density of the material. To measure this efficiency η_{sc}, the number of x-ray photons absorbed by the scintillator are compared to the number of incident photons:

$$\eta_{sc} = 1 - e^{\mu \cdot \rho \cdot d} \qquad (5.1)$$

In this equation μ equals the mass attenuation coefficient of the scintillator material, ρ, the density of the scintillator material, and d, the scintillator thickness. In contrast, the light emission efficiency of a scintillator depends on parameters such as the amount of light photons emitted per absorbed x-ray and the re-absorption or self-absorption attenuation of light photons in the scintillator material.

The resolution of a scintillating system is directly related to the scintillator thickness (Equation 5-1) because depth affects both the x-ray scatter and the direction of the emitted light. A thicker scintillator is more effective in detecting photons because a more powerful collecting area (thicker medium) is being used to intercept and record them. Thin screens allow some photons to pass completely through without passing any input to the image. However, thicker screens create a larger point spread function; a point at the entrance of the screen will cover a more extensive region of the output region of the screen. As a result, blurring occurs and the sharpness of the image is compromised.

5.4.2 LODOX breast imaging scintillator

The light sensitive scintillator material currently used in LODOX technology (Terbium doped Gadolinium Oxysulfide) is a green light emitting x-ray phosphor. The x-ray mass attenuation coefficient for Gadolinium Oxysulfide is shown below at various x-ray energies. At lower energies, the attenuation coefficient is substantially large, illustrating that a low energy x-ray source increases the absorption of photons in the scintillator. For this reason, Gd_2O_2S:Tb is a common material for clinical mammography scintillation. Gadolinium Oxysulfide is currently used for commercial mammography-specific x-ray screens, such as the Microvision® Detail or Microvision® Fast Detail green-emitting intensifying screens.

The mass attenuation coefficient for Gadolinium Oxysulfide is sufficiently high in the mammographic energy range (15-35keV). As a result, Gd_2O_2S:Tb is highly efficient at low energies. This composition is recommended by the author for a LODOX breast imaging system.

When LODOX breast phantom images were generated at low x-ray energies (40kV), visualization was poor because the scintillator thickness was selected for imaging with higher energy x-rays. A thinner LODOX scintillating screen could improve the conversion efficiency of absorbed x-rays to light by lessening the spread of light inside the screen. Unlike radiographic scintillators, the photon absorption efficiency in mammography screens may be as high as 50% due to low energy x-rays (Huda and Sloan, 1995). The thick LODOX screen also collects a large portion of low energy beams however, the conversion of these x-rays to light is reduced through the longer path length. As stated above, a thicker screen permits greater point spreading, contributing to blurring which is especially detrimental to small objects, such as microcalcifications, in breast tissue. Since the increased high energy photon collecting power of a thick screen is not required for the low energy photons used in mammography, a thin screen would reduce the amount of light spread from the point of photon absorption to the point of light detection. Thus, a scintillator created for the mammographic energy range, specifically in thickness, is predicted to powerfully improve low contrast imaging to optimize LODOX breast imaging.

5.5 Mechanical Considerations

5.5.1 Fundamental Parameters

There are a number of differences in the mechanics of the current LODOX system and a mammography system. The size and imaging capacity of the current LODOX-PPM is not practical for screening mammography. The machine is currently able to image an entire body, where only approximately $500cm^2$ need to be imaged for a mammogram. Thus, the number of CCD cameras used in the LODOX-MP system configuration (12) are excessive for such a small imaging area.

Similarly, the source to image receptor distance of the LODOX machine is approximately 1000mm, while SIDs in mammography range from 50-75cm, with 60-65cm being the most common (Wu *et al.*, 1991). This large relative distance is appealing because resolution is a direct function of SID. The penumbra (P), an outcome of geometric blurring, can be calculated from the focal size as the following:

$$P = \frac{T_w(H - H_0)}{H_0} \qquad (5.2)$$

T_w is the size of the actual focal spot, H, the source to detector distance, and H_0, the source to object distance. As stated in x-ray tube considerations, a penumbra results from a finite focal spot size. When photons reach the front of an object they cast a shadow on the detector plate as they diverge from the focal spot and cross one another. From the equation above, it is evident that the closer an object is placed to the detector, the smaller the penumbra effect.

However, aside from improved spatial resolution, the dimensions of the LODOX C-arm appears to be too bulky for a mammographic clinic setting. Thus, a balance between a largest possible SID, and the most convenient clinical size are important considerations for potential construction of such a device.

Mammography systems usually require a grid to maximize image quality by reducing scatter. LODOX technology does not utilize a grid however, its low scatter to primary ratio (0.2) is far below the range of standard mammography (0.6-1.0) (Huda and Slone, 1995). Likewise, scatter to primary ratios generated using equations of Boone *et al.* (2000) at particular breast thicknesses and diameters (0.29-0.59) were still higher than LODOX SPR. Although grids reduce scatter, they require a patient dose that is two to three times larger. For LODOX based breast imaging, a grid is not recommended because the minimal amount of scatter does not necessitate one.

5.5.2 Compression

Mammography systems are expected to be capable of generating 25-45lb of force (Kopans, 1998). However, the amount of pressure that a patient feels is dependent upon the size of her breast because this pressure is equal the force divided by the surface area over which the force is applied. Compression pain is the most common patient complaint in mammography.

For two-dimensional mammography imaging, compression is considered essential for reducing radiation scatter and increasing spatial resolution. Therefore, a potential LODOX breast imaging system may require the implementation of some form of a compression paddle, depending on whether or not other adjustments (a mammography specific tube and scintillator) create sufficient mammographic image quality alone.

Arguments also exist that suggest compression is not crucial for this particular system. For example, compression minimizes the effects of geometric sharpness yet, alternative methods (such as increasing the source to image detector distance) can be utilized for the same effect. Compression also improves contrast by diminishing scatter. However, the low scatter to primary ratio of scanning systems such as LODOX intimates that compression may not be necessary. Compression is also implemented because it reduces dose – which LODOX scanning technology also accomplishes. To ultimately determine the feasibility of compression elimination in LODOX-based breast imaging, many factors, such as focal spot blur, breast motion, and tissue overlap, must also be tested.

5.5.2 Three-dimensional LODOX mammography

Two-views are essential in breast cancer detection because the additional information from the cranio-caudal view allows for the cancer to be seen more easily on the oblique view (Hackshaw *et al.*, 2000). Studies have shown that a significantly higher number of cancers could be detected from two views versus one (24%) with a lower recall rate (15%) (Wald *et al.*, 1995). Although initial detection is also dependent upon the position, size, and type of cancer (Hackshaw *et al.*, 2000), the utilization of additional perspectives for data acquisition facilitates easier detection. In this respect, the depth perception added by imaging with a third dimension is an unforeseen advantage for both detection and diagnosis of breast cancer. For example, the overlapping of dense tissue in a conventional 2D scan can obscure lesions (Feig and Yaffe, 1998). Any objects that are located along the same x-ray beam path may be either partially or totally covered by one another.

Like other mammography systems that employ the use of a moveable arm, LODOX maintains a large number of available observation angles for imaging. With the C-arm, a radiologist can analyze any suspicious areas of the breast at multiple angles. This may be useful for future 3D breast reconstruction. With this in mind, a system that employs a bed with an opening for pendulant breast examination (such as that used in stereotactic biopsies) could introduce a non-compression mammography technique. Positional considerations for this proposition are listed below:

	Patient lying down	Patient sitting or standing
Anatomical effects	force of gravity stretches breast downward	slouched position makes breast more pronounced
Necessity for compression	dependent on image quality	dependent on image quality
CT capable	definite possibility (with appropriate equipment)	less possible
Face shield	trolley acts as natural face shield	face shield required
Angle flexibility	any desired imaging angle with C-arm rotation	CC and MLO images with 90° rotation of arm

Table 5.3: Preliminary parameter comparisons for reclined breast imaging system.

Appendix A
Beam Testing

For accuracy in HVL measurements, the entire sensitive region of the ionization chamber was covered by the X-ray beam. To ensure this, film screen x-rays were taken to determine the width of the beam at the detector. The width of the LODOX beam can be adjusted at the x-ray source with a collimator that ranges from 0.4 to 1.4 mm. These x-rays were also analyzed using a densitometer to determine the uniformity of the beam incident to the ionization chamber.

Using a KODAK X-Omat V therapy verification pack and two 18 x 26 cm films, the beam was exposed on standard radiographic film. The therapy verification envelopes act as a scintillating material and the x-ray was then developed using standard film processing technique. Each exposure was in the alignment mode, to imitate the method required for using the ionization chamber to collect LODOX-PPM data.

Films

For the first film, a 40kV x-ray beam was exposed at five separate locations (the closest adjustable kV to mammographic x-ray energy). The exposure time was varied at each location: 500ms, 1000ms, 1200ms, 2400ms, and 4600ms. Exposures at 1200, 2400, and 4600ms were generated to represent the amount of time needed to scan a breast with a diameter of 16cm at fast, medium, and slow scanning speeds (138mm/s, 69mm/s, and 34.5mm/s, respectively).

With the second film, the x-ray energy was set at 100kV, and the focal spot was varied (both large and small) at 500ms and 1000ms, to determine any beam width deviation due to resolution. 100kVs was selected for this because exposures of higher energies are clearer and easier to measure of a film. Exposure periods less than two seconds, along with compression, are desired for the reduction of motion blurring (Haus and Yaffe, 2000).

Beam uniformity

A densitometer (X-rite Company, Model 301, US Patent 4,080,075) was used to measure the film density of the resultant x-rays. After the equipment was nulled, five measurements were taken at periodic increments across the length of each beam, to determine the general uniformity of the density throughout the beam. The density of the beam at its center was of most interest because the ionization chamber is placed directly in the middle of the beam. Next, three density measurements were taken at the center of every beam exposure, each approximately a millimeter from the previous. The film density measured from the LODOX beam exhibits uniformity in the central region.

Exposure	Measured film density		
500ms	0.32	0.3	0.32
1000ms	0.44	0.44	0.44
1200ms	0.49	0.49	0.49
2400ms	0.74	0.74	0.74
4600ms	1.07	1.06	1.09

Table A.1: Uniform film density was measured across the width of a LODOX beam.

The first set of measurements, across the length of the beam, exhibited more variation in film density than measurements taken in the center of the beam. It was noted that exposures taken with the small focus demonstrated higher density, hence higher intensity, than those taken with the large focal spot.

Beam width

The second sets of measurements, taken at the beam center, were relatively consistent (as seen in Table A.2 on the right). The divergence at an exposure of 4600ms was again considered to be attributed to emulsion unevenness, or early exposure of the film to light, because the film was randomly darkened at this edge.

Exposure	**Energy**	**Focus**	**Beam Width**
500ms	40kV	Small	5.0mm
1000ms	40kV	Small	5.5mm
1200ms	40kV	Small	5.5mm
2400ms	40kV	Small	5.5mm
4600ms	40kV	Small	6.0mm
500ms	100kV	Small	6.0mm
1000ms	100kV	Small	6.0mm
500ms	100kV	Large	6.5mm
1000ms	100kV	Large	7.0mm

Table A.2: Summary of beam width. The beam must be larger than the ionization chamber diameter (5.2 mm).

The most useful measurement generated from the films, however, was the width of the beam at the surface of the table (where the ionization chamber is placed). According to the manufacturer specifications, the diameter of the ionization chamber is 5.2mm. This area must be completely covered to attain accurate measurements. As seen from Table A.2, the measured widths of the beam from film just fulfill this requirement. As a consequence of this preliminary experiment, a great significance was placed on the precise centering of the dose meter for exposure readings using digitally generated images.

Appendix B
Equations

Contrast

With LODOX technology, dark current subtraction, flat field normalization, and logarithmic conversion are applied to the data signals. The individual signals can be translated into a function of their intensity with the following equations (Booysen):

$$S_a = \frac{\log_{10}\left[\left(I_0 e^{-\mu_1 z_1}\right)/I_0\right]}{\log_{10}[1]} \tag{B.1}$$

$$S_b = \frac{\log_{10}\left[\left(I_0 e^{-\mu_2 z_2}\right)/I_0\right]}{\log_{10}[1]} \tag{B.2}$$

I_0 represents the input intensity, z quantifies the height above the detector, and μ_1 and μ_2 are the attenuation coefficients for the two blocks. The attenuation coefficient equates to the product of a material's attenuation coefficient per density, and the density of the object itself ($\mu=\alpha\rho$). For contrast purposes, the attenuation in free air can be assumed negligible.

By substituting density factors and equating the flat field intensity to the intensity at height z_2 above the detector, contrast can be reduced with the following derivation:

$$Contrast = \frac{z_1\mu_1 - z_2\mu_2}{z_1\mu_1 + z_2\mu_2} \tag{B.3}$$

Fourier Transform:

The general equation of a Fourier transform is made up of a real part, R(f), and an imaginary part, I(f), which can be illustrated as the following:

$$R(f) = \int_{-\infty}^{+\infty} \phi(x)\cos 2\pi * fxdx \tag{B.4}$$

$$I(f) = -\int_{-\infty}^{+\infty} \phi(x) i \sin 2\pi * fxdx \tag{B.5}$$

When measuring a rectangular pulse, a Fourier transform can be obtained by substituting $\phi(x)$ with k, which would yield the following equations:

$$R(f) = \frac{ka_0 \sin(\pi f a_0)}{\pi f a_0} \qquad I(f) = 0 \tag{B.6}$$

Theoretically, the function of a rectangular pulse (φx) with constant value k between negative $a_0/2$ and $a_0/2$, could be reconstructed from a Fourier transform similar to the illustration below:

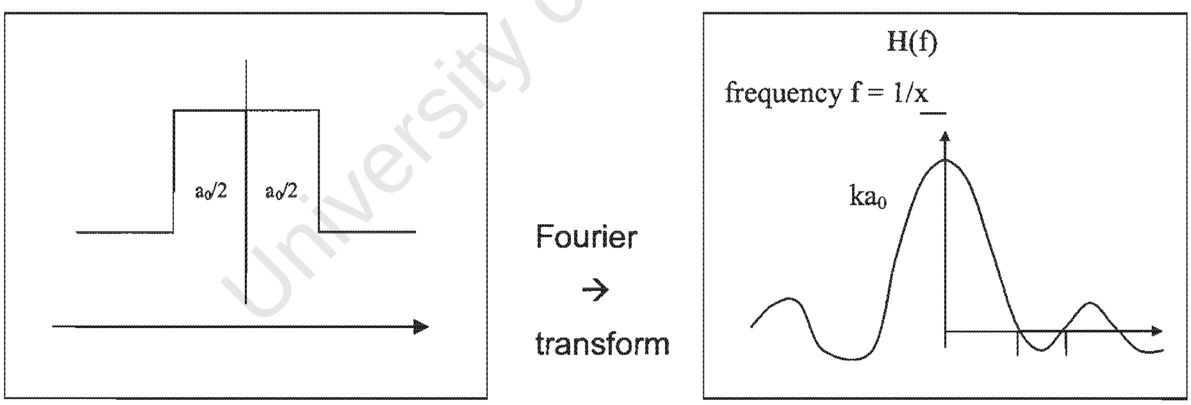

The Fourier transform equates the pulse, φx, to the sum of an infinite number of cosine functions (Johns and Cunningham, 1983). Mathematically, this integral can be represented as the following sum:

$$\psi(x) = 2\sum_{f_1}^{f_n} \frac{k}{\pi f} \sin(\pi f a_0)\cos(2\pi f x)\Delta f \tag{B.7}$$

Δf is equal to the frequency interval, which should be made small for an accurate calculation. This equation can be calculated using a computer program and describes the way a signal, such as that generated from the detector, is described by the MTF.

Signal to Noise Ratio

The amplitude of the signal is defined as the intensity difference between a specific region and its surrounding area:

$$S = I_a - I_b \qquad \text{(B-8)}$$

To quantify noise, one must calculate the standard deviation (σ) of the signals from their average intensity. The Root Mean Squared (RMS) of these values is the noise amplitude.

$$N = \sqrt{\sigma_a^2 + \sigma_b^2} \qquad \text{(B.9)}$$

Thus, the ratio of S:N is calculated as the following (Booysen, 1998):

$$\frac{S}{N} = \frac{I_a - I_b}{\sqrt{\sigma_a^2 + \sigma_b^2}} \qquad \text{(B.10)}$$

Calculating w(z)

The percentage absorption, $\eta(E)$, between E values of 10-145 keV is calculable with the following equation (Boone, 1992):

$$\eta(E) = \sum_{n=1}^{8} A_n E^n \qquad \text{(B.11)}$$

Calculating alpha and beta

Parameters alpha and beta have been modeled and listed by Gkanatsios and Huda for large-scale diagnostic radiology (between 50-140kV, and at 5-30cm in thickness). For mammography, x-ray energy is usually below 40kV. The data tables created by Gkanatsios and Huda can be extrapolated to verify the agreement of mammographic calculations for w(z). It is noted that these values are calculated for a 5cm phantom thickness. With this technique, the energy imparted at 40kV, with the measured LODOX HVL of 1.59 mm of Al, is 3.17E-14J/(R*cm^2).

In the calculations of Huda and Gkanasios, alterations in the anode angle (from 6 to 20 degrees) had a minor impact on the value of energy imparted to the system. At a given tube voltage and HVL, the value of w(z) changed less than 2% for changes in tube anode angle. The anode angle for LODOX technology employs an x-ray tube with an anode angle that falls between these parameters at an angle of 7 degrees.

Appendix C
Noise (Signal to Noise Ratio)

Noise of an imaging system can be quantified through a comparison of the useful image information to random signal variations. In a digital system, this erratic variability is a result of quantum and electrical noise, and can have a strong degenerative effect on image quality. Thus, noise is the sum of the total random signals that interfere with the transmitted x-ray signal. Degradation of image quality, and limited visualization of low contrast objects, results from excess noise. A majority of noise in radiographic images derives from the fundamental quantum nature of x-ray photons.

There are a number of parameters used to measure noise. The first, the noise power spectrum (NPS), is a graph of how the variance of the image signal is distributed over spatial frequency. Essentially this is an indicator of the noise level itself. The signal to noise ratio (SNR) of the image describes the relative magnitude of noise in comparison to the magnitude of useful image signal. The square root of the SNR, the noise equivalent quanta (NEQ), is termed as such because it represents the number of x-ray quanta that the system *seems* to be using to produce the resultant image. Since the SNR and NEQ describe the information content of the image, increases in both surmise greater consistent detail and distinction from background noise. The quality of image for different size details can be described by analyzing either the SNR or NEQ with respect to the spatial frequency. Detective quantum efficiency (DQE) measures the system's ability to transfer information (including noise) from the entrance of the image receptor to the displayed image. This parameter is the ratio of the NEQ at the entrance of the image receptor over the NEQ at the final image. Whilst the NEQ indicates the quality of an image, its DQE designates the system's ability to generate that quality, which is subject to the MTF, NPS, and the number of incident x-ray quanta at the receptor.

The SNR describes the relative magnitude of noise to the useful imaging signal. The amplitude of the signal is defined as the intensity difference between a specific region and its surrounding area. To quantify noise, one must calculate the standard deviation

(□) of the signals from their average intensity (I). The Root Mean Squared (RMS) of these values is the noise amplitude. Thus, the ratio of S:N is calculated as the following:

$$\frac{S}{N} = \frac{I_a - I_b}{\sqrt{\sigma_a^2 + \sigma_b^2}} \qquad \text{(C.1)}$$

A system's ability to detect an object requires the largest signal to noise ratio (SNR) possible, especially for small, low-contrast objects. The square of the SNR value is thus equated to the number of x-ray quanta that the system uses to produce the image, the NEQ (noise equivalent quanta). A larger SNR or NEQ implies that more subtle details can be detected over the noise.

Appendix D

Literature Data

Energy (keV)	*% Interactions by Each Process* Coherent	Compton	Photoelec	*% Energy Transferred* Compton	Photoelec
10.0	4.5	3.1	92.4	0.1	99.9
15.0	8.5	10.8	80.7	0.4	99.6
20.0	11.6	23.3	65.1	1.3	98.7
30.0	13.0	50.7	36.3	6.8	93.2
40.0	11.0	69.6	19.4	19.3	80.7
50.0	8.6	80.4	11.0	37.2	62.8
60.0	6.8	86.6	6.6	55.0	45.0

Table D.1: Types of photon interactions in water (Johns and Cunningham, 1983).

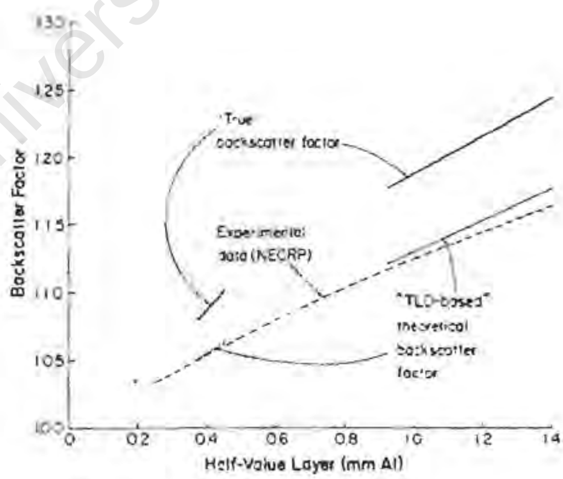

Figure D.2: Comparison of Backscatter Factors (BSF) generated by Doi and Chan through Monte Carlo simulations, and actual measured BSFs (with thermoluminescent dosimeters).

Figure 7

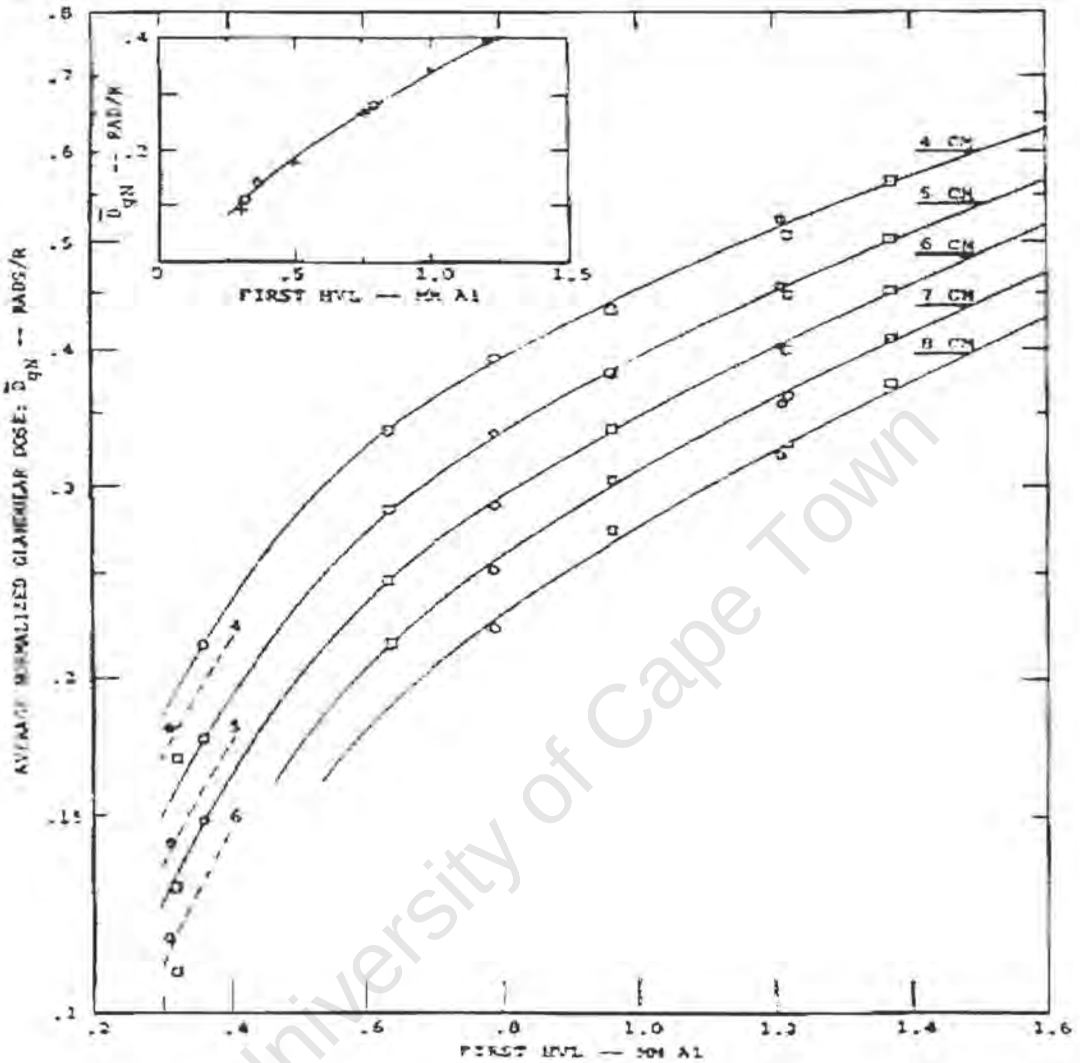

Figure D.3: Mean glandular dose conversion factors (rad/Roentgen) based on half value layer. Data is taken from Stanton *et al.* , Figure 7 (1984)

Appendix E
Current Mammography System Approaches

The worldwide mammography market was predicted to surpass the $500 million mark by the year 2004 (Klucas, 2000). As of July 2000, four relatively unique styles of digital mammography systems were being tested for commercial use.

The first system, developed by Fisher Imaging (Denver, CO), is a slot-scanning digital mammography unit. As an x-ray beam scans across the breast laterally, a synchronized detector moves along an arc across the chest wall behind the breast. The x-ray beam is well collimated and restricted to a slot that is approximately 24 x 1.4 cm. The detector, with the same dimensions, is composed of a thallium-activated cesium iodide phosphor fiberoptically coupled to a charge coupled device (CCD) with approximately 2000 columns and 256 rows. The charge produced in the CCD is shifted down the columns at a rate equal to the motion of the slot beam and detector. This process, called time delay integration (TDI), reduces artifacts caused by motion and stitching because the signal from a particular path through the breast is integrated in the CCD. The signal is not read out and digitized until the last row of the CCD. This system shares the most similarities with LODOX imaging systems. LODOX also involves line scanning and images using CCD technology (12 CCD cameras) and TDI.

The General Electric Medical Systems unit is an amorphous silicon photodiode array consisting of 1,800 x 2,300 100micrometer elements in a solid-state flat panel. A thin uniform layer of cesium iodide phosphor lies on top of the panel so that each photodiode in the matrix is light sensitive. In response to light emission from the phosphor surface, the charge produced on each diode element activates a thin-film transistor switch that is connected to a series of control lines and data lines. Readout trigger pulses are sent sequentially to each row of elements and the electrical charge on the lines connecting each column of elements is digitized. The GE detector is modified to fit into a conventional mammography Bucky assembly.

In the large area mosaic system developed by Trex Medical (currently a Lorad product), a cesium iodide scintillator (18 x 24 cm) is coupled to a 3 x 4 array of CCDs with 12 demagnifying fiberoptic tapers. The 12 detector modules create subimages that are stitched together by a bonding technique to create a seamless image of the breast. The entire detector is composed of 6,400 x 4,800 elements that measure 40 micrometers on each side and, like the GE unit, can be retrofitted on the company's conventional mammography unit.

The fourth system, devised by Fuji (Stamford, CT), utilizes a photostimulable phosphor to store the transmitted radiation. Europium doped barium fluorochloride is an x-ray stimulable phosphor material that acts as the x-ray absorber. The traps in the crystalline material of the phosphor store the electronic charges created by the x-rays based on the amount of incident radiation. For example, more traps are filled when a higher level of radiation is absorbed. The flat phosphor plate detector is then removed after exposure and scanned with a helium neon laser beam which discharges the traps. As a result, blue light is emitted from the detector. Finally, a photomuliplier tube collects and measures the blue light to form a digitally actualized image.

Siemens Medical Solutions, Sectra Imtec, DALSA, and Instrumentarium Imaging are also currently in the process of developing full field digital mammography technology. These systems offer variations of the digital mammography devices described above, and are described by the Radiological Society of North America (RSNA) as "works-in-progress" (as of June 2001). Many of these digital mammography systems are being clinically tested at the current time.

Appendix F
Equipment

Figure F.1: Universal Unidos Dosemeter, Manufactured by PTW (Freiburg). A similar apparatus (Model 10002; Serial number 20001) was used for all exposure readings, and hence dose calculations in this study. Likewise, exposure readings were necessary in calculating LODOX half value layers.

Figure F.2: 0.02cc Ionization Chamber, Manufactured by PTW (Freiburg). This apparatus (Model W 23342; Serial number 948) was attached to the dosemeter above for all exposure readings.

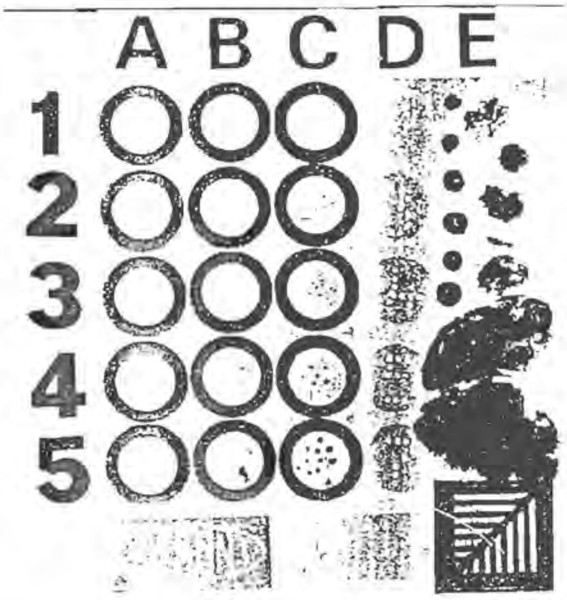

Figure F.3: Dupont mammography phantom layout. Row A contains microcalcifications ranging from 83-250μm in diameter, Row B contains fibers ranging from 0.3-0.8mm in diameter, Row C contains spheres and nodules ranging from .35-1.08mm in diameter, Row D contains detail disks ranging in thickness from 0.2-0.75mm, and Row E contains simulated tissues and structures. This phantom is not accredited by the American College of Radiology.

References

http://cope.uicc.org/Updates/breastcancer.shtml (Breast Cancer Worldwide)

http://www.cansa.org.za/ (Cancer Association of South Africa)

http://marathon.csee.usf.edu/Mammography/Database.html (University of Southern Florida Mammography Database)

Ackerman LV, Gose EE: Breast lesion classification by computer and xeroradiography. *Cancer* 30: 1025-35, 1972.

Andolina VF, Lille SL, Willison KM *Mammographic Imaging: A Practical Guide.* J.B. Lippincott Company, Philadelphia; 1992.

Bankman IN, Christians-Barry WA, Kim DW: Automated recognition of microcalcification clusters in mammograms. *Proc SPIE* 1905:731, 1993

Barnes GT, Brezovich IA. The Intensity of Scattered Radiation in Mammography. *Radiology* 126:243-247, 1978.

Baydush, AH, Floyd, CE: Improved image quality in digital mammography with image processing. *Medical Physics* 27(7): 1503-1507, 2000.

Beningfield SJ, Potgeiter JH, Bautz P, Shackleton M, Hering E, de Jager G, Bowie G, Marshall M, Cox G, Pagliari G, Coetzee N: Evaluation of a new type of direct digital radiography machine, *South African Medical Journal* 89(11): 1182-1188, 1999.

Boice JD, Land CE, Shore RE: Risk of breast cancer following low-dose radiation exposure. *Radiology* 131:589-95, 1979.

Boone JM, Cooper VN: Scatter/primary in mammography: Monte Carlo validation. *Medical Physics* 27(8):1818-31, 2000.

Boone JM, Lindfors KK, Cooper VN, Seibert JA: Scatter/primary in mammography: Comprehensive results. *Medical Physics* 27(10): 2408-2416, 2000.

Booysen A: LODOX ADM Image Quality Review and Specification. DebTech Documentation, 1998.

Cheng HD, Lui YM, Freimanis RI: A novel approach to microcalcification detection using fuzzy logic technique. *IEEE Trans Med Imaging* 17:442-50, 1998.

Curry TS, Dowdey JE, Murry RC, *Christensen's Physics of Diagnostic Radiology*, 4th ed. ; Lea & Febiger, Philadelphia, 1990.

Diagnostic X-ray Imaging Task Group No. 7: *Equipment Requirements and Quality Control for Mammography.* American Institute of Physics, AAPM Report No. 19. 1990.

Doi K, Chan H-P. Evaluation of absorbed dose in mammography: Monte Carlo simulation studies. *Radiology* 135: 199-208, 1980.

Dobbins JT, Ergun DL, Rutz L, Hinshaw DA, Blume H, Clark DC: DQE(f) of four generations of computed radiography acquisition devices. *Medical Physics* 22, 1581-1593, 1995.

Dubuque GL, Cacak RK, Hendee WR. Backscatter factors in the mammographic energy range. *Medical Physics* 4 (5): 397-399, 1977.

Egan R. Experience with mammography in a tumor institute evaluation of 1,000 studies. *American Journal of Roentgenology* 75: 894-900, 1960.

European Commission of Quality Assurance for Mammographic Standards, 1996.

Feig SA. Estimation of currently attainable benefit from mammography screening of women aged 40-49 years. *Cancer* 75: 2412-2419; 1995.

Feig SA, Haus AG, Jans RG. Mammography – A User Guide [NCRP Report no.85] (Vol 85). Bethesda, MD: National Council on Radiation Protection and Measurements, 1986.

Feig SA, Yaffe MJ. Digital mammography. *RadioGraphics* 18:893-901; 1998.

Fullerton GD, Kopp DT, Waggener RG, Webster EW (editors). *Biological Risks of Medical Irradiations.* American Institute of Physics; New York: 1980.

Good W, Sumkin J, Ganott M: Detection of masses and clustered microcalcifications on data compressed mammograms. *American Journal of Roentgenology* 175; 1573-1576, 2000.

Gkanatsios NA, Masters thesis: Computation of Energy Imparted in Diagnostic Radiology, Master of Science in Diagnostic Medical Physics, University of Florida Gainesville, FL. Chapters 3 and 4, p 1-18; 1995.

Gkanatsios NA, Huda W: Computation of energy imparted in diagnostic radiology. *Medical Physics* 24(4): 571-9, 1997.

Granfors PR, Aufrichtig R. "DQE(f) of an amorphous silicon flat panel x-ray detector: detector parameter influences and measurement methodology," *Proceedings of SPIE* 3977, p 2-13, 2000.

Granfors PR, Aufrichtig R. Performance of a 41x41-cm^2 amorphous silicon flat panel x-ray detector for radiographic imaging applications. *Medical Physics* 27(6): 1324-31; 2000.

Hackshaw AK, Wald NJ, Michell MJ, Field S, Wilson ARM: An investigation into why two-view mammography is better than one-view in breast cancer screening. *Clinical Radiology*, 55: 454-458, 2000.

Hammerstein GR, Miller DW, White DR, Masterson ME, Woodard HQ, Laughlin JS: Absorbed radiation dose in mammography. *Radiology*, 130: 485-491, 1979.

Hannon D. "Implementing Digital: The DR industry looks to standardize DQE measurement procedures" In: *Medical Imaging*: Health Tech Publishing Company, Inc. November, 2000.

Harris CH. "Digital Mammography Reaches Its Stride" In: *Medical Imaging*: Health Tech Publishing Company, Inc., p 36-42, May, 2001.

Haus, AG: State-of-the-art screen-film mammography: A technical view. *In* Barnes GT, Frey DG (eds): *Screen-Film Mammography: Imaging Considerations and Medical Physics Responsibilities.* Madison, WI, Medical Physics Publishing, 1991.

Haus AG, Metz CE, Chiles JY, Rossman K: The effects of x-ray spectrum from molybdenum and tungsten target tubes on image quality in mammography. *Radiology* 118(3): 705-9, 1976.

Haus AG, Yaffe MJ: Screen-film and digital mammography: image quality and radiation dose considerations. *Radiologic Clinics of North America* 38(4): 873-897, 2000.

Hendrick RE, Berns EA: Optimizing mammographic techniques. *In* Haus AG, Yaffe MJ(eds): *A Categotical Course in Physics: Physical Aspects of Breast Imaging. Syllabus.* Oak Brook, IL, Radiological Society of North America, 1999.

Huda W, Bissessur K: Effective dose equivalents, HE, in diagnostic radiology. *Medical Physics* 17(6): 998-1003, 1990.

Huda W, Slone R: *Review of Radiologic Physics.* Lippincott Williams & Wilkins; Philadelphia, 1995.

International Commission on Radiotion Units and Measurements (ICRU) Report 46. Photon, Electron, Proton and Neutron Interaction Data for Body Tissues. Bethesda, Maryland; February 1992.

International Electrotechnical Commission (IEC) Working Group 33. Characteristics of digital X-ray imaging devices – Determination of the detective quantum efficiency, Committtee Draft: 62B/416/CD, 2000.

Johns HE, Cunningham JR. *The Physics of Radiology, Fourth Edition.* Charles C. Thomas Publisher; Springfield, Illinois (USA): 1983.

Kopans DB, *Breast Imaging, Second Edition.* Lippincott-Raven, Philadelphia; 1998.

Klucas, G. "The State of Mammography" In *Medical Imaging*: Health Tech Publishing Company, Inc., p126-132, November, 2000.

Lewin JM, Hendrick RE, D'Orsi CJ, Isaacs PK, Moss LJ, Karellas A, Sisney GA, Kuni CC, Cutter GR. Comparison of full-field digital mammography with screen-film mammography for cancer detection: Results of 4,945 paired examinations. *Radiology* 218: 873-880, 2001.

Malkin D, Li FP, Strong LC, Fraumeni JF, Nelson CE, Kim DH, Kassel J, Gryka MA, Bischoff FZ, Tainsky MA. Germ line p53 mutations in a familial symptom of breast cancer, sarcomas, and other neoplasms. *Science* 250: 1233-1238, 1990.

Mettlin C. Global breast cancer mortality statistics. *Cancer J Clin.* 49:138-144, 1999.

Mettler FA, Upton AC, Kelsey CA, Ashby RN, Rosenburg RD, Linver MN. Benefits versus risks from mammography: a critical assessment. *Cancer* 77: 903-909, 1996.

Morrison AS, Brisson J, Khalid N. Breast cancer incidence and mortality in breast cancer detection demonstration project. *Journal of the National Cancer Institute* 80(19):17-24, 1998.

Morishita J, Doi K, Bollen R, Bunch PC, Hoeschen D, Sirand-rey G, Sukenobu Y. Comparison of two methods for accurate measurement of modulation transfer functions of screen-film systems. *Medical Physics* 22, 193-200; 1995.

Moskowitz M. Breast Imaging. In: Donegan WL, Spratt JS eds. *Cancer of the Breast.* Philadelphia: Sanders; 206-239, 1995.

Nishikawa RM, Giger ML, Doi K, Vyborny CJ, Schmidt RA: Computer-aided detection of clustered microcalcifications on digital mammograms. *Med Bio Eng Comput* 33:174-8, 1995.

Nishikawa RM, Yaffe MJ: Signal-to-noise properties of mammographyic film screen systems. *Medical Physics* 12:32-9, 1985.

Park JM, Choi HK, Bae SJ, Lee MS, Ahn SH, Gong G: Clustering of breast microcalcifications: revisited. *Clinical Radiology* 55: 114-118, 2000.

Peters ME, Voegeli DR, Scanlan KA. *Handbook of Breast Imaging.* Churchill Livingstone Incorporated; London, 1989.

Preston DL, Kato H, Kopecky KF, Fujita S: Studies of mortality of atomic bomb survivors. Cancer mortality 1950-1982. *Radiation Research* 11:151-78, 1987.

Rajan G. *Advanced Medical Radiation Dosimetry.* Prentice-Hall of India Private Limited; New Delhi: 1992.

Reynolds HE. Advances in breast imaging. *Hemotol Oncol Clinics of North America* 13:333-48, 1999.

Rossman K: Spatial fluctuations of x-ray quanta and the recording of radiographic mottle. *American Journal of Roetgenology* 90:863-9, 1963.

Samei E, Flynn M. A method for measuring the presampled MTF of digital radiographic systems using an edge test device. *Medical Physics* 25(1), 102-113; 1998.

Shrivastava PN. Radiation dose in mammography: An energy-balance approach. *Radiology* 140: 483-490, 1981.

Shaw R. The equivalent quantum efficiency of the photographic process. *The Journal of Photographic Science* 11:199-204,1963.

Sickles EA. Breast calcifications: mammographic evaluation. *Radiology* 160: 289-293, 1986.

Sivaramakrishna, R. Obuchkowski, N., Chilcote, W., et al. Comparing performance of mammographic enhancement algorithms: a preference study. *American Journal of Roentgenology* 175; 45-51, 2000.

Spiesberger W: Mammogram inspection by computer. *IEEE Trans Biomed Eng* 26:213-9; 1979.

Stanton L, Villafana T, Day J, Lightfoot DA. Dose evaluation in Mammography. *Radiology* 150: 577-584, 1984.

Tabar L, Fagerberg G, Chen H. Efficacy of breast cancer screening by age: new results from the Swedish Tow-Country Trial. *Cancer* 75: 2507-2517, 1995.

Tokunaga M, Land CE, Yamamoto T, Asano M, Tokuoka S, Ezaki H, Nishimori I: Incidence of female breast cancer among atomic bomb survivors, Hiroshima and Nagasaki, 1950-1080. *Radiation Research* 112:243-72, 1987.

Vyborny, Carl, Giger, Maryellen, Nishikawa, Robert, Computer-Aided detection and diagnosis of breast cancer. *Radiologic Clinics of North America* 38: 725-739, 2000.

Vyborny C, Schmidt RA: Technical image quality and the visibility of mammographic detail. *In* Haus A, Yaffe MJ (eds): Syllabus of Categorical Course on Technical Aspects of Mammography. Oak Brook, IL, Radiological Society of North America, p103, 1994.

Wald, NJ, Murphy P, Parkes C, Townsend J, Frost C. UKCCCR multicentre randomized controlled trial of one and two view mammography in breast cancer screening. *British Medical Journal* 311: 1189-1193, 1995.

Wanebo HH, Huvos AG, Urban JA: Treatment of minimal breast cancer. *Cancer* 33:349-57, 1974.

Webster E: Mammary cancer induction by low doses of x-rays. *In* Logan WW, Muntz EP (eds): Reduced Dose Mammography. New York, NY, Masson Publishing USA, Inc., 1979.

Wells, P.N.T. (ed). *Scientific Basis of Medical Imaging*. Churchill Livingstone; Edinburgh: 1982.

Whitlock JP, Evans AJ, Burrell SE, Pinder SE, Ellis IO, Blamey RW, Wilson AR: Digital imaging improves Upright stereotactic core biopsy of mammographyic microcalcifications. *Clinical Radiology* 55:374-7, 2000.

Williams MB, Fajardo LL, Otto GP, Tran JM: Evaluation of a Prototype Detector for Full Breast Digital Mammography with CCDs and Modified Schmidt Camera Optics. *Radiology Society of North America* (online pubication: http://ej.rsna.org/EJ_0_96/0020-96.fin/ms.htm); 1997.

Wooster R, Neuhausen SL, Mangion J. Localization of breast cancer susceptibility gene, BRCA2, to chromosome 13q12-13. *Science* 265:2088-2090, 1994.

Wu X, Barnes GT, Tucker DM, Spectral depedence of glandular tissue dose in screen film mammography. *Radiology* 179: 143-148, 1991.

Yaffe MJ (eds): Syllabus of Categorical Course on Technical Aspects of Mammography. Oak Brook, IL, Radiological Society of North America, 1994.

Yaffe MJ, Hendrick RE, Feig SA, Rothenberg LN, Och J, Gagne R: Recommended specifications for new mammography equiptment: Report of the ACR-CDC focus group on mammography equipment. *Radiology* 197:19-26, 1995.

Yaffe MJ, Taylor KW, Johns HE. Spectroscopy of diagnostic x-rays by a Compton-scatter method. *Medical Physics* 3(5) : 328-334, 1976.